Journal of Colloid and Interface Science 702 (2026) 138823

Contents lists available at ScienceDirect

Journal of Colloid And Interface Science

journal homepage: www.elsevier.com/locate/jcis

Validation of a lipopeptide approach to a safe-and-sustainable-by-design strategy on TiO_2 nanoparticles UV filters

Elena Cesa [a], Anna Luisa Costa [b], Lara Faccani [b], Dario Fornara [c], Hulya Yilmaz [d], Mustafa Culha [d], Sevin Adiguzel [d], Gulnur Sener [d], Nilay Cicek [d], Tugba Muhlise Okyay [d], Paola Ziosi [e], Sébastien Artous [f], Sébastien Jacquinot [f], Arantxa Ballesteros [g], Javier Alcodori [g], Ivone Pinheiro [h], Laura Rodriguez-Lorenzo [h], Begoña Espiña [h], Filippo Marchetti [a], Anna Baldisserotto [a], Stefano Manfredini [a,*], Silvia Vertuani [a]

[a] *Faculty of Medicine, Pharmacy and Prevention, Department of Life Sciences and Biotechnology, University of Ferrara, Via L. Borsari 46, 44121 Ferrara, Italy*
[b] *CNR-ISSMC (former ISTEC), National Research Council of Italy, Institute of Science, Technology and Sustainability for Ceramics, Via Granarolo 64, 48018 Faenza, Italy*
[c] *Lamberti SpA, Albizzate, Italy*
[d] *Sabanci University Nanotechnology Research and Application Center, Istanbul, Turkey*
[e] *Ambrosialab srl, Via Mortara 171, 44121 Ferrara, Italy*
[f] *University Grenoble Alpes, CEA, Liten, DTNM, 38000 Grenoble, France*
[g] *ITENE, Valencia, Spain*
[h] *International Iberian Nanotechnology Laboratory, Avenida Mestre José Veiga, 4715-330 Braga, Portugal*

GRAPHICAL ABSTRACT

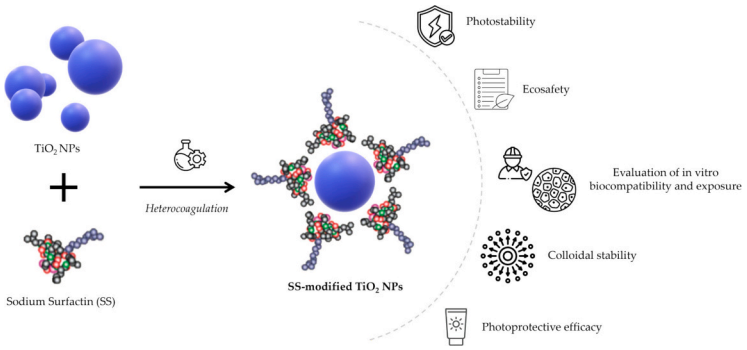

* Corresponding author.
E-mail addresses: cselne@unife.it (E. Cesa), anna.costa@issmc.cnr.it (A.L. Costa), lara.faccani@issmc.cnr.it (L. Faccani), dario.fornara@lamberti.com (D. Fornara), mustafa.culha@sabanciuniv.edu (M. Culha), sevin.adiguzel@sabanciuniv.edu (S. Adiguzel), gulnur.sener@sabanciuniv.edu (G. Sener), nilay.cicek@sabanciuniv.edu (N. Cicek), tugba.okyay@sabanciuniv.edu (T.M. Okyay), paola.ziosi@ambrosialab.com (P. Ziosi), sebastien.artous@cea.fr (S. Artous), Sebastien.Jacquinot@cea.fr (S. Jacquinot), arantxa.ballesteros@itene.com (A. Ballesteros), javier.alcodori@itene.com (J. Alcodori), ivone.pinheiro@inl.int (I. Pinheiro), laura.rodriguez-lorenzo@inl.int (L. Rodriguez-Lorenzo), begona.espina@inl.int (B. Espiña), filippo.marchetti@unife.it (F. Marchetti), anna.baldisserotto@unife.it (A. Baldisserotto), smanfred@unife.it (S. Manfredini), vrs@unife.it (S. Vertuani).

https://doi.org/10.1016/j.jcis.2025.138823
Received 26 April 2025; Received in revised form 13 August 2025; Accepted 24 August 2025
Available online 25 August 2025

ARTICLE INFO

Keywords:
Titanium dioxide nanoparticles
Surfactin
Safe-and-sustainable-by-design
Self-assembling
Multi-techniques characterization
Phototoxicity
Free radical
Biosurfactant

ABSTRACT

Titanium dioxide nanoparticles (TiO_2 NPs) are well suited for cosmetics and polymer films because they efficiently absorb UV light while remaining transparent to visible light. Their widespread use requires strategies for managing potential human and environmental risks. Implementing the Safe and Sustainable by Design (SSbD) methodology to advanced chemicals and materials is a major global challenge and a concept that is included in several EU research projects. This study employed a SSbD strategy by functionalizing the surface of TiO_2 nanoparticles with a lipopeptide-based biosurfactant (Sodium Surfactin, SS). A colloidal heterocoagulation approach was used to produce SS-modified TiO_2 nanoparticles. Different design options (TiO_2 source, order of addition, TiO_2/SS weight ratio) were investigated, and the properties were compared by measuring the UV filtering capability, photoreactivity, dustiness index, biological and ecotoxicological endpoints. This allowed us to estimate the safety and sustainability profile in agreement with the steps suggested by the JRC SSbD framework. The lipopeptide-based coating was essential for managing UV light-induced photoactivity and significantly lowering both in vitro cytotoxicity and ecotoxicity while simultaneously enhancing photostability when applied in cosmetic formulations. These results demonstrate that a colloidal process, which can be easily scaled up for industrial purposes, is a promising and exploitable SSbD strategy for the design and implementation of TiO_2 NPs based UV filters.

1. Introduction

The rapid advancement of nanotechnology has led to the widespread use of engineered nanomaterials (ENMs) in various industrial and consumer applications owing to their unique properties at the nanoscale. Titanium dioxide (TiO_2) nanoparticles (NPs) are one of the most widely studied and utilized ENMs with applications in pigments, coatings, cosmetics, sunscreens, and photocatalysts. However, the properties that make TiO_2 NPs desirable, such as their high surface-area-to-volume ratio, as well as their photoelectric and photochemical properties, also contribute to their potential toxicity [1]. Understanding these dual aspects is crucial for balancing their safe use in consumer products and industrial applications with potential risks to human health and the environment [2]. Biological effects and cellular response mechanisms have been extensively discussed in many studies [3]. Human exposure to TiO_2 NPs can occur through ingestion, dermal absorption, or inhalation, during both the manufacturing process and their application in products. One of the most accredited ways TiO_2 nanoparticles can cause toxicity is through the production of reactive oxygen species (ROS) [4] or the adsorption and transport of bioactive molecules [5]. This can lead to oxidative stress, inflammation, genetic damage, changes in metabolism, and possibly, cancer. The amount and type of cell damage depend on the characteristics of the TiO_2 nanoparticles, such as their size, crystal structure, and photoactivation [6,7]. The ROS-forming ability is crucial for photocatalytic activity, but it is also relevant for dark catalytic phenomena [8,9]. On the other side, TiO_2 NPs can have positive health impacts by mitigating the exposure to ultraviolet (UV) radiation and the consequent skin alterations: TiO_2 nanoparticles' absorption and scattering contribute to the overall UV rays attenuation more efficiently than microparticles [10], enhance the Sun Protection Factor (SPF), and provide better protection against photodamage [11]. However, its dual reactivity to sunlight presents challenges in the sunscreen industry, as light absorption can activate the catalyst, leading to redox reactions between the photoinduced charges (see Fig. 1) and other components within the sunscreen formulation. Therefore, owing to their extensive use and debated potential toxicity, strategies to mitigate the harmful effects of TiO_2 NPs on humans and non-target organisms have emerged as new areas of investigation. Surface modifiers for TiO_2 NPs, both inorganic and organic, are among the most explored solutions. However, only few strategies have been developed and validated so far [12–15].

In response to these concerns, the European Commission's Green Deal and Chemicals Strategy for Sustainability has emphasized the importance of designing materials that are inherently safe and sustainable throughout their life cycle (Safe-and-Sustainable-by-Design approach, SSbD). This approach is particularly relevant for nanomaterials, where early-stage interventions can significantly mitigate potential risks [16]. In the framework of the European projects SBD4Nano and SUNRISE, we therefore developed and tested a safe-by-molecular-design strategy by modifying the surface of TiO_2 nanoparticles with a biosurfactant to suppress their photocatalytic activity and improve their dispersibility in a cosmetic matrix. This modification aims to enhance the environmental and health profiles of TiO_2 NPs while preserving their functional properties. Among the possible surface modifiers, we leveraged our concurrent studies on the use of the cyclic lipopeptide biosurfactant sodium surfactin (SS), a multifaceted biometabolite arising from sustainable sources (i.e., food waste and agricultural by-products), owing to its wide range of beneficial activities,

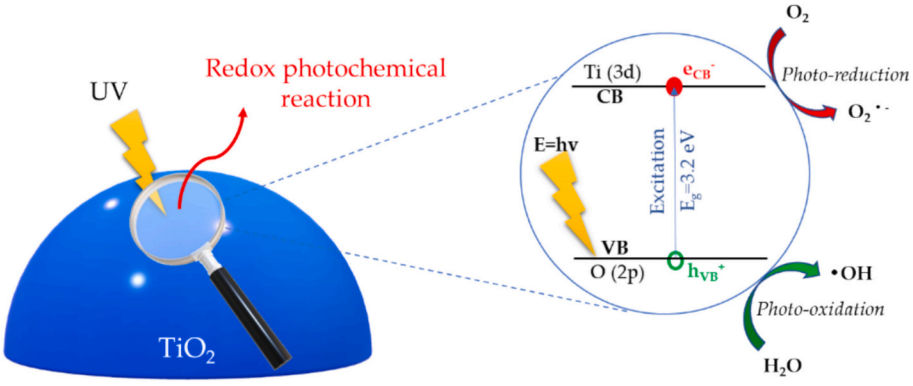

Fig. 1. Photoactivated surfaces and mechanism of TiO_2 photocatalysis. Briefly, the three basic steps of photocatalytic reactions are: 1) photoexcitation of charge carriers, 2) charge carrier separation and diffusion to the photocatalyst surface, and 3) oxidation and reduction reactions on the catalyst surface.

easy biodegradability and environmentally friendly nature [17–19].

As an emerging surface-active molecule secreted by various strains of *Bacillus subtilis*, SS offers the possibility of adsorption on solid surfaces as a result of its amphiphilic naturem which strongly affects the properties of the substrate particles, characterized by a low critical micelle concentration (CMC) value of 0.0003 %, 3000 times more effective in reducing the surface and interfacial tensions than lecithin (natural product), and 300 times more effective than SDS (sodium dodecyl sulfate).

The unique structure of SS includes a hydrophilic cyclic peptide part constructed by seven amino acids (L-Glu, L-Leu, D-Leu, L-Val, L- Asp, D-Leu, L-Val). Of these, two acidic and five hydrophobic residues are closed by a lactone bound and attached to a hydrophobic hydrocarbon chain of varying lengths and branching [20]. The Structure-property relationship known as the "Horse saddle" folding mode of surfactins is reported in Fig. S1 [21].

2. Materials and methods

2.1. Chemicals

Aeroxide® P25 (P25) (Evonik Industries AG, Essen, Germany), Eusolex® T-AVO (EU) (cosmetic regulation approved, Merck KGaA, Darmstandt, Germany), Sodium Surfactin (SS) (Ambrosialab, Ferrara, Italy), the undissociated form of SS (SCOOH) was obtained by treating SS with Dowex® 50Wx8 cationic exchanger resin (Merck KGaA, Darmstandt, Germany), Acid Blue 9 (AB9) (purity ≥99 %, Farmalabor, Milan, Italy). All other chemicals used in this study were of analytical grade.

2.2. Design of modified TiO_2 NPs

A colloidal self-assembly approach [22–24] was applied to modify the surface of TiO_2 NPs with SS.

The design involved dispersing titanium dioxide NPs powders (P25 or EU) in ultrapure water (UW) or EtOH (concentrations from 10 to 30 mM) through sonication to separate loosely agglomerated particles. The SS or SCOOH solutions were mixed with the TiO_2 suspensions, and the reaction mixture was sonicated for 30 min. The flask was wrapped in tinfoil to avoid photocatalytic reactions, and the suspension was magnetically stirred for 24 h at 60 °C under reflux conditions. At the end of the reaction, the TiO_2-SS mixtures were centrifuged at 6000 rpm for 30 min at +4 °C to promote pellet deposition. Finally, the pellet was washed twice with UW, the residual unbound SS war removed and then lyophilized for 72 h.

The resulting samples, depending on the order of addition (first, the component into which the second component was dripped), were named P25@SS, SS@P25, EU@SS, and SS@EU, respectively (Table 1).

Different stoichiometric ratios of materials and solvents were evaluated during a preliminary screening phase, and the most appropriate weight ratio was selected to accurately reflect the experimental conditions and to promote a ligand exchange reaction between the hydroxylated nanoparticle surface and the functionalizing ligands. Ultrapure water and ethanol were deliberately employed as environmentally benign solvents to reduce the toxicity associated with conventional organic solvents, while ensuring chemical compatibility. These choices were strategically made to minimize the presence of unbound material in the final dispersion and to reduce overall waste generation, aligning the functionalization process with principles of safety and sustainability.

2.3. Characterization

2.3.1. Colloidal behavior: DLS and ELS

The colloidal properties of sample-based suspensions were investigated in terms of hydrodynamic diameter (dDLS) and zeta potential (ζ-potELS) determined by dynamic and electrophoretic light scattering measurements, respectively, using a Zetasizer Nano ZSP (model ZEN5600, Malvern Instruments, UK).

Analyses of colloidal samples were performed at 25 °C on powders dispersed in UW with ultrasonic mixing for 10 min to obtain a final concentration of 320 μg/mL (320 ppm). After a 2-min temperature equilibration step, 1 mL of samples for DLS and 700 μL of samples for ELS were measured consecutively three times, and data were obtained by averaging the three measurements. Acid-base titrations were performed to assess the pH at the isoelectric point (pH i.e.p) [25]. The titrants used were 0.1 M KOH and 0.1 M HCl solutions on 0.1 wt% suspensions, diluted with distilled water.

2.3.2. Surface characterization: FTIR-ATR spectroscopy

Surface analysis of the obtained samples was performed using a

Table 1
Details of the reaction variables applied to each compound during the optimization phase of the colloidal approach.
Colloidal characterization results of starting and modified materials diluted in UW at 25 °C. The composite samples are named, indicating the addition of the component into which the second component was dripped and the weight ratio between the two components in brackets.

a)

Modified materials	Dripped solution	Solvent of reaction	Stoichiometry	$[mM]_{TiO2}$	$[mM]_{ligand}$
P25@SS (1:1)	SS	UW	1:1	15,8 mM	15,8 mM
SS@P25 (1:1)	P25	UW	1:1	15,8 mM	15,8 mM
P25@SS (2:1)	SS	UW	2:1	30 mM	15 mM
SS@P25 (2:1)	P25	UW	2:1	15 mM	30 mM
P25@SS (1:1)	SS	Et0H	1:1	15,8 mM	15,8 mM
SS@P25 (1:1)	P25	Et0H	1:1	15,8 mM	15,8 mM
EU@SS (1:1)	SS	UW	1:1	17,4 mM	17,4 mM
SS@EU (1:1)	EU	UW	1:1	17,4 mM	17,4 mM
EU@SS (1:1)	SS	Et0H	1:1	17,4 mM	17,4 mM
SS@EU (1:1)	EU	Et0H	1:1	17,4 mM	17,4 mM
SS@EU (10:1)	EU	Et0H	10:1	9,4 mM	94,4 mM
P25@SCOOH (1:1)	SCOOH	UW	1:1	15,8 mM	15,8 mM
SCOOH@P25 (1:1)	P25	UW	1:1	15,8 mM	15,8 mM

b)

Optimized materials	**Dripped solution**	**Solvent of reaction**	**Weight ratio**	**$[mM]_{TiO2}$**	**$[mM]_{ligand}$**
P25@SS (13,2 wt%)	SS	UW	7,6:1	3,16 mM	1,6 mM

Fourier-transform infrared spectrometer equipped with a diamond Attenuated Total Reflectance accessory (FTIR-ATR).

The prepared samples (P25@SS (1:1) and EU@SS (1:1), as well as P25, EU, and SS alone) were analyzed in dry form. ATR Spectra were recorded in transmission mode, carrying out a total of eight scans for powder samples at room temperature (25 °C) with a spectral resolution of 4 cm^{-1}, using Resolution Pro software version 2.5.5 (Agilent Technologies, USA). Scanning was carried out in the range 4000–550 cm^{-1} to identify the main functional groups.

2.3.3. Structural characterization: XRD spectroscopy

The X-Ray diffraction (XRD) spectra were obtained with a Bruker D8 Advance X - ray diffractometer, using CuKα monochromatic radiation (1.5406 Å). The instrument was equipped with a particular fast detection system (Accelerator), capable of providing spectra with a better signal/noise ratio than normal detectors in a few seconds of acquisition. The samples were analyzed in the 2Θ range 5°–80°.

2.3.4. Morphological characterization: SEM-EDS and TEM analysis

The chemical composition and surface particle morphologies were investigated using scanning electron microscopy (SEM) (Model EVO 40, DE) coupled with a detector for energy-dispersive X-ray spectroscopy (EDS) (Inca Energy 300, Oxford Instruments). The samples were examined at acceleration voltage of 15–20 kV.

To improve the surface conductivity of the samples and consequently the image resolution, 7 nm layer of gold sputtering deposition treatment was applied through vacuum evaporation. The images were collected under high vacuum and with a high electron beam voltage to achieve maximum resolution. EDS system analysis was used to verify the presence of organic coating through elemental analysis/composition, in a "spot mode" in which the beam was localized on a single area manually chosen within the field of view.

2.4. Thermal analysis: TGA and DSC

The thermal behavior was investigated by thermogravimetric analysis (TGA) and differential scanning calorimetry (DSC) using a Netzsch STA 449 F3 Jupiter® instrument. Measurements were performed on sample powders weighing approximately 6 mg and placed in a platinum/rhodium crucible using alumina (Al_2O_3) for internal calibration. The Experiment was conducted in an air/N_2 mixture (40 mL/min of air and 80 mL/min of N_2) at a heating rate of 5 °C/min from room temperature to 900 °C.

2.5. Photocatalytic activity

The photocatalytic activity of the TiO_2-based samples was determined by adapting the method previously described by van Driel et al. [26], monitoring the degradation of a water-soluble synthetic food dye used in analyses as an indicator (AB9) following UV radiation. The dye degradation test was then prepared by adding 10 mg of photocatalytic material to 7,7 μM ethanolic solution of AB9, at a final volume of 100 mL, and properly sonicated for 10 min to uniformly disperse the powder in the AB9 solution. The experiment was conducted with magnetic stirring at room temperature in a UV box equipped with a UV-A lamp (Osram, L BLUE UVA 18 W/78, wavelength) at 20 cm from the sample. The wavelength of the emitted light was in the range UVA 315–400 nm, with an irradiation power of 4.7 W and an intensity of 7800 cd.

After exposure, the samples (2 mL) were centrifuged at 8500 rpm for 5 min using an Eppendorf centrifuge at room temperature, filtered (0.45 μm) to separate the powder from the dye solution, and subsequently analyzed by UV–Vis spectrophotometry. The analysis was carried out measuring the AB9 solution at $\lambda_{max} = 630$ nm using a UV–vis spectrophotometer (UV-6300PC, VWR, Milan, Italy). The concentration of AB9 was evaluated according to a calibration curve, and the results are expressed in terms of dye depletion efficiency (%) by Eq. (1), which indicates the ratio between the amount of reagent consumed (dye depleted) and the amount of reagent initially present in the reaction environment, according to the Lambert-Beer law, where A0 is the initial absorbance and Af is the final absorbance:

$$Dye\ depletion\ efficiency\ (\%) = (A0 - Af\ )/A0 \times 100 \quad (1)$$

2.6. Dustiness index: vortex shaker method

The dustiness of TiO_2-based powders was investigated using the innovative Vortex Shaker method (the experimental configuration is reported in Fig. S2, [27]) at high emissions to simulate real handling scenarios.

The data were evaluated using two parameters derived from the respirable filter sampling and CPC (Condensation Particle Counter) measurements:

- Mass-based Dustiness Index (DI_{RM}) measured in mass (mg/kg).
  It is defined as the mass Δm_f of particles collected on a respirable sampling filter divided by the mass M_0 of powder placed in the cylindrical tube (Eq. (2))

$$DI_{RM} = \left(\Delta m_f\right)/M_0 \quad (2)$$

- Number-based Dustiness Index (DI_{RN}) measured in number (#/mg). It is defined as the number of particles emitted over the duration of the vibrating period (t_V) by the mass M_0 of powder placed in the cylindrical tube (Eq. (3))

$$DI_{RN} = \frac{1}{M_0}\sum_0^T \frac{(C_{CPC}(t)^* Q_{VS}{}^* \Delta t_{CPC}}{t_V} \quad (3)$$

Adapting a test protocol previously reported in the literature [28], the test samples were prepared by pouring 0.5 cm^3 of powder into an Eppendorf® microtube. After filling, tubes were weighed to the nearest 10 μg. The samples were conditioned for at least 24 h prior to the dustiness test in a laboratory-made humidity-controlled chamber at 50 ± 5 % RH. After cleaning the entire test bench and/or, if necessary, changing the tubing and connections, and having equipped the cyclone with a pre-weighed filter for gravimetric analysis, the airflows were checked using a flow calibrator. The cleanliness of air through the test bench was assessed using CPC measurements. The mass of test sample M_0 was obtained from the difference between the mass of the filled microtube and the mass of the microtube after emptying.

The Vortex Shaker method can also be used to determine the specific surface areas of powders with a single point by the Brunauer-Emmett-Teller (BET) analysis method, in which samples are pre-treated under vacuum at 120 °C.

2.7. Ecotoxicity

2.7.1. Freshwater alga and cyanobacteria, growth inhibition test OECD 201 (algae tests)

The ecotoxicity of different nanomaterials was evaluated using OECD TG 201 in *Selenastrum capricornutum*. The medium used for the growth of algae and during the test was designed in the EPA Method 1003.0.

ENMs were dispersed in artificial freshwater, the medium where the organism grows. The dispersion conditions were optimized and compared with the ENMs dispersed in UW (modified and non-modified) based on the NANoREG dispersion method. No stabilizers were used in this study. The dispersion method involves estimating the volume of the UW to redisperse the nanomaterial at the desired concentration. Then, the powder was weighed into a well-cleaned vial/flask selected and dispersed using the UW estimated in the first step to reach the desired concentration (not recommended to be more than 2.56 mg/ml). For optimal dispersion, 1 mL UW was added while shaking for 1 min. After 1

min of incubation, the rest of the volume was added under shaking until the desired concentration. Finally, the vial/flask was placed in a container with ice water, and the dispersion was sonicated for at least 5 min. To prepare the ice water mixture, a 250 mL glass beaker was filled with ice and placed upside down in an insulation box. As soon as the volume of ice reached 10–15 % of the glass beaker, the vial was placed inside the beaker to keep the dispersion cold during sonication. The sonication time and conditions must be adjusted depending on the sonicator employed in each lab according to the NANoREG protocol.

Three replicates of the alga were exposed for 72 h to nanomaterials dispersed in freshwater. The nominal concentrations used were 100, 10, 1, 0.1, 0.01, and 0 mg/L. The growth of the alga was estimated by measuring the Optical Density at 670 nm (OD670). The OD of the algal suspensions was measured during the three days of the test, i.e., after 24 h, 48 h and 72 h. Data treatment was performed using the MOSAIC tool for ecotoxicologists and regulators designed by the University of Lyon and using Bayesian statistics. An ENM was considered toxic when the effective concentration 50 (EC50), that is, the concentration at which the population was halved, is under 100 ppm. In the case of the algae, it will be considered as EC50 the population where the growth is halved. IC95 values for each treatment can be consulted in tables SX, SY and SZ.

2.7.2. Zebrafish embryotoxicity test (ZET)

In this ecotoxicity test, we evaluated the toxicity of nanomaterials on zebrafish embryos by following and adapting the OECD 236 (zebrafish embryos tests) freshwater organism.

Zebrafish spawning and eggs assortment was performed as previously described [29]. Embryotoxic effects were assessed at different developmental stages of zebrafish [30], in an adaptation of OECD test guideline 236. Ten viable zygotes per replicate (well) were arbitrarily transferred to a 24-well plate, and waterborne exposed (in a semi-static regime) to the serial diluted nominal concentrations of 0, 0.01, 0.1, 1, 10, and 100 mg/L of NPs and 13,2 mg/L of the biomolecule (SS), concentration of the SS in a 100 mg/L dispersion of the NPs, until 80 h post-fertilization (hpf). Pre-filtered freshwater was defined as the experimental control. Four replicates of the test concentrations were screened in two independent experiments. Two milliliters per well (replicates) was used. The stability of the particles was characterized using a size analyzer (SZ-100 device, Horiba, ABX SAS, Amadora, Portugal).

Particles were dispersed in the media for the assay (freshwater) and compared with a dispersion in UW. The dispersion stability was studied immediately after dispersion (0 h) and at the maximum incubation time during the ZET assay (24 h). P25@SS was dispersed at a concentration of 100 mg/L using an ultrasound bath at 37 Hz and 100 % power for 30 min. P25 NPs were dispersed using a 1:1 ratio of humic acid as stabilizer and 30 min probe sonication at 50 % amplitude in pulses of 30 s on and 10 s off. NPs test concentrations were first dispersed, and the pH was verified at the lowest and highest nominal concentrations to ensure a tolerable environment to for normal embryonic development in zebrafish [30]. NPs test concentrations were pre-heated at 26 ± 1 °C each day before the assay, and the plates were exposed to the same photoperiod as the spawning tank. One experiment was acknowledged as “valid” with an embryonic lethality threshold set at 10 % of the experimental control. At 8, 32, 56, and 80 hpf, different age-correspondent embryonic developmental events were investigated. Embryos were observed and photographed using a Nikon Eclipse Ts2 inverted microscope coupled with a Nikon DS-Fi3 camera. Survival was checked at all hpf. Tests on fish embryonic stages were conducted at the International Iberian Nanotechnology Laboratory (INL) (Braga, Portugal) as an adaptation to the FET test (OECD test guideline 236), as defined at the Council of Europe Directive 86/609/EEC on the protection of experimental animals, setting the regulatory limit of exposure at the free-living stage (that is, at the end of embryogenesis). As the last endpoint tested preceded this developmental age, the provisions of the directive did not apply. Therefore, a ratified ethical consent was not required. A concentration of 100 mg/L was considered as the highest test (nominal) concentration of NPs, according to OECD test guideline 203, which states the limit for the testing of chemicals in this range.

Statistical analysis was performed using JASP free software. For multiple comparisons, one-way ANOVA followed by Tukey’s post hoc test was employed, while the Kruskal-Wallis test with Dunn’s post hoc test was used for non-normally distributed data. Statistical significance was set at $P < 0.05$.

2.8. Preliminary assessment of in vitro toxicity in BEAS-2B, RAW264.7, and HSF cell lines

Cell viability was measured using Cell Counting Kit-8 (WST-8) and Alamar Blue assays on human bronchial epithelial cells (BEAS-2B), mouse alveolar macrophage cell line (RAW264.7) from a tumor induced by Abelson murine leukemia virus, and human skin fibroblasts (HSF).

Colorimetric WST-8 (for BEAS-2B and RAW264.7) and Alamar Blue (for HSF) kits were purchased from Sigma-Aldrich. In the WST-8 assay, the amount of formazan dye formed was directly related to the metabolic activity of cells. Similar to the WST-8 assay, Alamar Blue (resazurin assay) was used to evaluate cell proliferation by measuring dehydrogenase activity within cells. When detected, resazurin, a blue dye with low fluorescence, is reduced to resorufin, a highly fluorescent red dye. The assays were performed according to the manufacturer’s instructions.

Before the cell viability studies, dispersion studies of NPs in different aqueous media, including ultrapure water (UW), phosphate buffer saline (PBS), and Dulbecco’s Modified Eagle Medium (DMEM), were conducted using an ultrasonic bath at increasing time points in order to find well-dispersed conditions without damaging the structure of NPs. As a result, DMEM was found to be the best choice for cell culture. The NPs were dispersed in DMEM at a higher concentration and diluted to lower concentrations for in vitro analysis. The cells were seeded in transparent 96-well plates and exposed NPs with increasing concentrations (1–10–100–200 μg/mL) at different times (6–24 h). Cells were then washed twice with PBS 1× and incubated in fresh medium with 10 % WST-8 reagent for 3 h. Subsequently, 80 μL aliquots of the media with developed color were transferred into new 96-well plates to eliminate the interference from NPs and NPs taken up by the cells (80 μL were transferred instead of 100 μL to prevent bubble formation, which interferes with the absorbance measurement). The absorbance of each well with WST-8 reagent was measured at 450 nm (690 nm was used as the reference wavelength and subtracted) in a microplate reader (iMark™, Bio-Rad, UK). Results are reported as relative WST-8 activity, where 1.0 corresponds to the absorbance measured in the control cultures.

Each condition was tested in triplicate per experiment, and all experiments were independently repeated at least three times ($n = 3$). Negative control was set to 100 % proliferation. Data are expressed as mean ± standard deviation (SD). Statistical differences between the treated groups and controls were evaluated using one-way ANOVA followed by Tukey’s post hoc test, with $p < 0.05$ considered statistically significant, as determined by ORIGIN 2025. Treatments were considered statistically significant if $p \leq 0.05$ (represented by *). The non-significance level is not shown.

2.9. Evaluation of sun protection efficacy in vitro

2.9.1. Emulsion preparation

To evaluate the filtering parameters, we designed a cosmetic formulation scheme (Table S1) for an oil-in-water (O/W) emulsion on which we tested P25@SS compared to P25 and SS alone.

More specifically, the emulsions were designed considering the functionalization data of the P25@SS product obtained by TGA measurement (weight loss of approximately 10 wt%), from the total amount of UV filter in the formulation of 10 % to have the same concentration of P25 in both formulations.

Briefly, the aqueous phase (Phase I) and oil phase (Phase II) were set up separately. Phase II was heated at about 65 °C to promote melting of the components, while Phase I involved preheating the UW (70 °C) at which time the components were added starting with solvation of xanthan gum, using a Turboemulsifier Silverson® L5M-A (Silverson®, Evry, France) until fully dispersed. When both phases were homogeneous and at an appropriate temperature (70 °C), emulsification was carried out by pouring Phase I flush into Phase II under Turboemulsifier Silverson® L5M-A agitation until a homogeneous product was obtained. Thereafter, it was allowed to reach room temperature under gentle stirring, and having reached 30–40 °C, it was finished by adding phase VI and III with the aid of Polytron™ PT1200E Handheld Homogenizer (Kinematica, Malters, Switzerland).

2.9.2. Determination of SPF

In vitro SPF analysis of the formulation was conducted using a method recently proposed by our research group, adapting the ISO 24443:2012 standard for the determination of UVA protection in vitro to UVB [31] and the requirements of European recommendation EC 647/2006 of September 22, 2006, on the efficacy evaluation of sunscreen products [32]. The method is based on the spectrophotometric evaluation of UV absorbance (calculated from transmittance) using a SHIMADZU UV-2600 spectrophotometer equipped with an integrating sphere ISR 2600 60 mm and coupled with SPF determination software (SPF calculator software version 2.1, Shimadzu, Milan, Italy), with emission wavelengths from 290 to 400 nm and 1 nm increments. Irradiation of each sample was executed using the Atlas SUNTEST CPS+ solar simulator (Suntest CPS; Atlas, Linsengericht, Germany), equipped with a xenon lamp, an optical filter to eliminate wavelengths shorter than 290 nm, and an IR-block filter to prevent thermal effects, and configured to operate between 40 and 200 W/m^2 in accordance with the ISO 24443:2012 procedure. For the investigation, four plates were prepared for five measurements. Results with covariance less than 3 % were deemed acceptable, and the following values were obtained post-irradiation:

i. SPF related to erythema-inducing radiation is calculated as described in Eq. (4):

$$in\ vitro\ SPF = \frac{\int_{\lambda=290nm}^{\lambda=400nm} E(\lambda)I(\lambda)d(\lambda)}{\int_{\lambda=290nm}^{\lambda=400nm} E(\lambda)I(\lambda)10^{-A(\lambda)}d(\lambda)} \quad (4)$$

where E(λ) is the erythema action spectrum (CIE-1987) at a wavelength λ, I(λ) is the spectral irradiance received from the UV source at λ, A(λ) denotes monochromatic absorbance per plate before UV exposure of the test product layer at λ and d(λ) the λ step (1 nm);

ii. SPF label UVAPF (UVA protection factor), described from the absorption spectra after irradiation by the following Eq. (5):

$$UVAPF = \frac{\int_{\lambda=290nm}^{\lambda=400nm} P(\lambda)I(\lambda)d(\lambda)}{\int_{\lambda=290nm}^{\lambda=400nm} P(\lambda)I(\lambda)10^{-A(\lambda)C}d(\lambda)} \quad (5)$$

where I(λ), A(λ), d(λ) are defined by Eq. X, P(λ) is the PPD (Persistent Pigment Darkening) action spectrum and C is the coefficient of adjustment the calculated in vitro SPF value to the labelled (in vivo) SPF value (recommended between 0.8 and 1.2). The UVA protection factor (UVAPF) of each sunscreen formulation was instrumentally verified before and after a period of controlled UV irradiation.

iii. SPF label/UVAPF ratio, based on the formula's performance in protecting specifically in the UVA range, relative to the overall SPF value declared on the label. Similarly to the Critical Lambda, this ratio provides an evaluation of the amplitude of the protection across the UV spectra without considering the magnitude of the filtering activity. Values approaching 1 are indicative of a broad-spectrum activity.

iv. SPF λ critical, which describes the amplitude of the protection across all the UV spectra (280–400 nm). It is defined as the wavelength at which 90 % of the area under the absorbance curve (AUC) is reached starting from 290 nm.

3. Results

3.1. Physicochemical characterization techniques

3.1.1. Colloidal properties

To assess the colloidal stability, the hydrodynamic diameter (dDLS), the zeta potential (ζ -potELS) at natural pH and the pH i.e.*p* values of both the pristine materials and TiO_2-modified samples were measured in UW and are reported in Table 2. As already confirmed in previous

Table 2
Colloidal characterization of the starting materials and SS-modified samples at 25 °C. The table reported the data in terms of hydrodynamic diameter (dDLS) in nm, PdI, Zeta Potential (ζ-potELS) in mV, natural pH and pH i.e.p. of both pristine materials and TiO_2-based nanosuspension. SS coating on P25 surfaces is the most promising "colloidal self-assembling method", which exploits oppositely charged nanoparticles.

Starting materials	Solvent of reaction	dDLS [nm]	PdI	ζ-potELS [mV]	Natural pH	pH i.e.p.
Aeroxide (P25)		599 ± 50	0,5	+ 41,1	3,7	6,13
Eusolex T-AVO (EU)		724 ± 30	0,4	−42,3	7,8	2,98
Sodium Surfactin (SS)		1852 ± 131	0,8	−48,5	6,4	< 2
Surfactin (SCOOH)		1653 ± 36	*n. d.*	0	5	2,4
Modified materials (molar ratio)						
P25@SS (1:1)	UW	241 ± 8	0,3	−30,3	6,2	3,07
SS@P25 (1:1)	UW	289 ± 39	0,4	−37,8	5,9	2,75
P25@SS (2:1)	UW	173,7 ± 19	0,3	−24,0	5	2,99
SS@P25 (2:1)	UW	843 ± 357	0,7	−47,0	5,5	< 2
P25@SS (1:1)	EtOH	2049 ± 687	1	−28,7	6,1	*n.d.*
SS@P25 (1:1)	EtOH	2368 ± 422	0,5	−21,6	5,5	*n.d.*
EU@SS (1:1)	UW	224 ± 6	0,3	−27,2	4,9	3,1
SS@EU (1:1)	UW	259 ± 59	0,3	−39,5	5,7	3,07
EU@SS (1:1)	EtOH	274 ± 4	0,3	−29,3	9,1	*n.d.*
SS@EU (1:1)	EtOH	227 ± 3	0,3	−39,1	7	*n.d.*
SS@EU (10:1)	EtOH	890 ± 50	0,4	−63,0	6,5	3,43
P25@SCOOH (1:1)	UW	1334 ± 108	*n. d.*	−51,0	5	1,9
SCOOH@P25 (1:1)	UW	2560 ± 881	*n. d.*	−24,0	5,5	2,1
Optimized materials (weight ratio)						
P25@SS (13,2 wt %)	UW	315 ± 8	0,4	−24,8	6,8	4,3

studies, DLS analysis of suspended P25 NPs showed a particle size distribution of about 600 nm, thus highlighting the strong tendency of TiO_2 to form large agglomerates in aqueous media [12].

The P25@SS (1:1) compound dispersed in water showed the smaller hydrodynamic diameters in comparison with pristine P25 and EU powders, despite the order of addition, most likely resulting from the steric hindrance and the electrostatic stabilization due to a sufficiently high negative ζ-potential, provided by the SS component. P25@SS samples in EtOH or in the excess of SS are characterized by big agglomerates most likely due to the compression of the electrical double layer in organic solvent or to a depletion coagulation effect due to excess SS [33]. By reducing the amount of SS (data not shown) we identified the minimum amount of SS providing a good colloidal stability and considered the sample P25@SS, with a content of 13,2 wt% SS vs. TiO_2 as the optimized sample.

The increase in the hydrodynamic diameter is observed in SCOOH-coated samples obtained from self-assembly method with undissociated surfactin. This is due to the absence of electrostatic stabilization provided by the uncharged SCOOH surfactin. By comparing the pH i.e.p (isoelectric point, the point of zero charge) values of P25 and SS (Fig. 2), we identified a pH range in which the two components had opposite charges (from 2 to 6), promoting heterocoagulation between the two phases [34]. As confirmation of the presence of SS surrounding the TiO_2 surface, we observed a shift in the SS pH i.e.p. toward a more acidic pH. Taking all the data into account, we decided, for practical reasons, to continue the characterization with the two samples P25@SS (SS 13,2 wt %) and EU@SS (1:1), both dispersed in ultrapure water (hereafter simply referred to as P25@SS and EU@SS), which represent the optimal compromise between a lower tendency to form aggregates and higher colloidal stability compared to P25 and EU, respectively.

As shown Fig. 3, the dispersion stability of the particles was observed over 3 days; all samples, including the control, showed relatively homogenous dispersion, indicating that the particles or emulsions were initially well mixed. In particular, the SS@EU and P25@SS samples seemed to have good initial dispersion. P25 appeared as a well-dispersed suspension, while SS formed clear solutions, indicating that both substances were initially well-dispersed. After 8 h, SS@EU and P25 showed good stability with no visible phase separation or sedimentation. This suggested that these formulations could maintain their dispersed state for a moderate period. However, SS and P25@SS began to show signs of slight sedimentation or aggregation, indicating the onset of instability in these samples after 3 days. SS@EU and P25 maintained a visually homogeneous appearance over 3 days without noticeable sedimentation, indicating macroscopic dispersion stability.

. This indicates that P25, probably in its nanoparticulate form, is stable in the medium and does not aggregate or settle even after prolonged exposure to UV conditions.

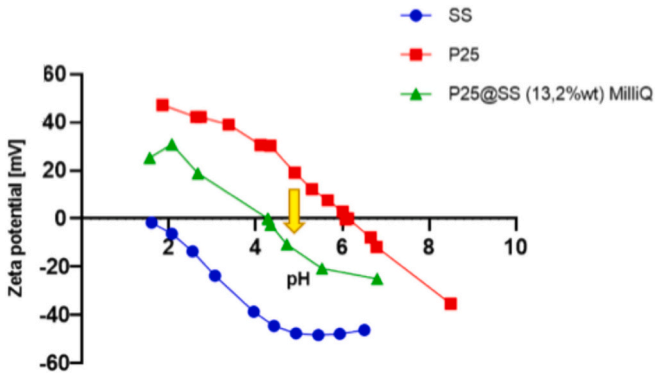

Fig. 2. Zeta Potential vs. pH curves of P25, SS, and P25@SS (SS 13,2 wt%) composite samples.

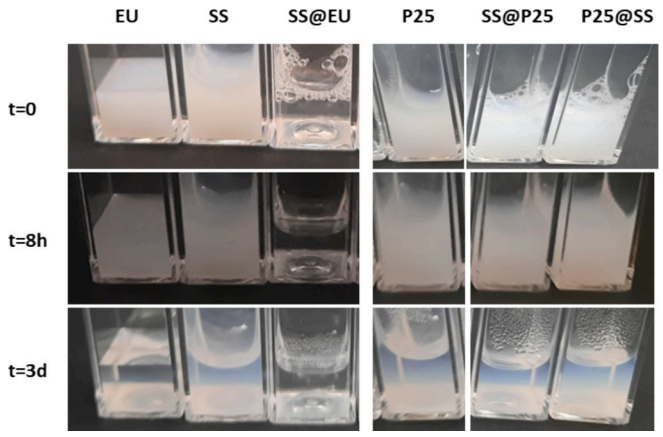

Fig. 3. Dispersion stability of various formulations, including EU, SS, P25, and combinations such as SS@EU, SS@P25, P25@SS, over time. Images were taken at three time points: immediately after preparation ($t = 0$), after 8 h ($t = 8$ h), and after 3 days ($t = 3$d).

3.1.2. *FTIR-ATR analysis*

Structural analysis and a basic peaks assignment were performed on FTIR-ATR spectrum, to characterize the SS "coating" on nano powder samples, specifically to investigate any changes occurring on the secondary structure of SS.

Fig. 4 shows a sequence of the spectra obtained on powders of P25, EU, SS, P25 coated with SS (P25@SS) and EU coated with SS (EU@SS). Specifically, the contributions from TiO_2, lipopeptide backbone, and lipopeptide headgroup can be observed and assigned. Because all the spectra of each group of SS-based treated samples exhibited similar features, a representative example is reported for P25@SS (Fig. 4A) and EU@SS (Fig. 4B).

The IR spectrum of SS clearly indicated characteristic peaks of peptides at 3290 cm^{-1} (N—H stretching mode), 1535 cm^{-1} (N—H bending mode and C═O stretching for Glu1 and Asp5), and 1645 cm^{-1} resulted from the stretching mode of the CO-N bond. Furthermore, the bands at 2956–2927 cm^{-1} and 1467–1368 cm^{-1} are representative of C—H group vibrations, confirming the presence of aliphatic chains (CH_3; CH_2) with symmetric stretching at 2871 cm^{-1}. About the lactonic ring, a characteristic peak at 1736 cm^{-1} as C═O stretching (carbonyl group of the cyclic ester) was observed. The pattern of the IR analysis confirms the cyclic nature of lipopeptide, and the characteristics of lipopeptide biosurfactant previously described [35].

The spectrum of P25 (blue line in Fig. 4A) showed the broadest band at 3352 cm^{-1} (O—H stretches) and a second weak band around 1630 cm^{-1} corresponding to the bending modes of water Ti-OH [36].

Indeed, regarding the IR spectrum of P25@SS (black line in Fig. 4a), some discriminations of the peaks representing the amide bonds (N-C=O) and, in general, the peptide ring were observed compared to pristine SS. For instance, a different ratio between the bands at 1651 cm^{-1} (C═O stretching of Amide *I*), 3289 cm^{-1} (NH_2 stretches), and 1735 cm^{-1} were shown.

The C—H vibrations remained almost unchanged for bands at 2956, 2927 and 2871 cm^{-1} except for a different profile of peaks from 1500 to 1300 cm^{-1}, corresponding to C—H and C—N bending vibrations. These modifications are possible owing to the hydrogen-bonding nature, confirming possible interaction of SS with the surface of TiO_2 NPs.

In addition, a different pattern was observed in the bands of the fingerprint region (1200–600 cm^{-1}) of P25@SS. This region is notable for a large number of infrared bands (including C—O, C—C and C—N single bond stretches, C—H and N—H bending vibrations, also out of plane) but is the most confusing region to interpret. Overall, additional peaks to P25 alone were recorded for P25@SS owing to the presence of SS and a possible rearrangement of its in the interaction with the surface of TiO_2 NPs.

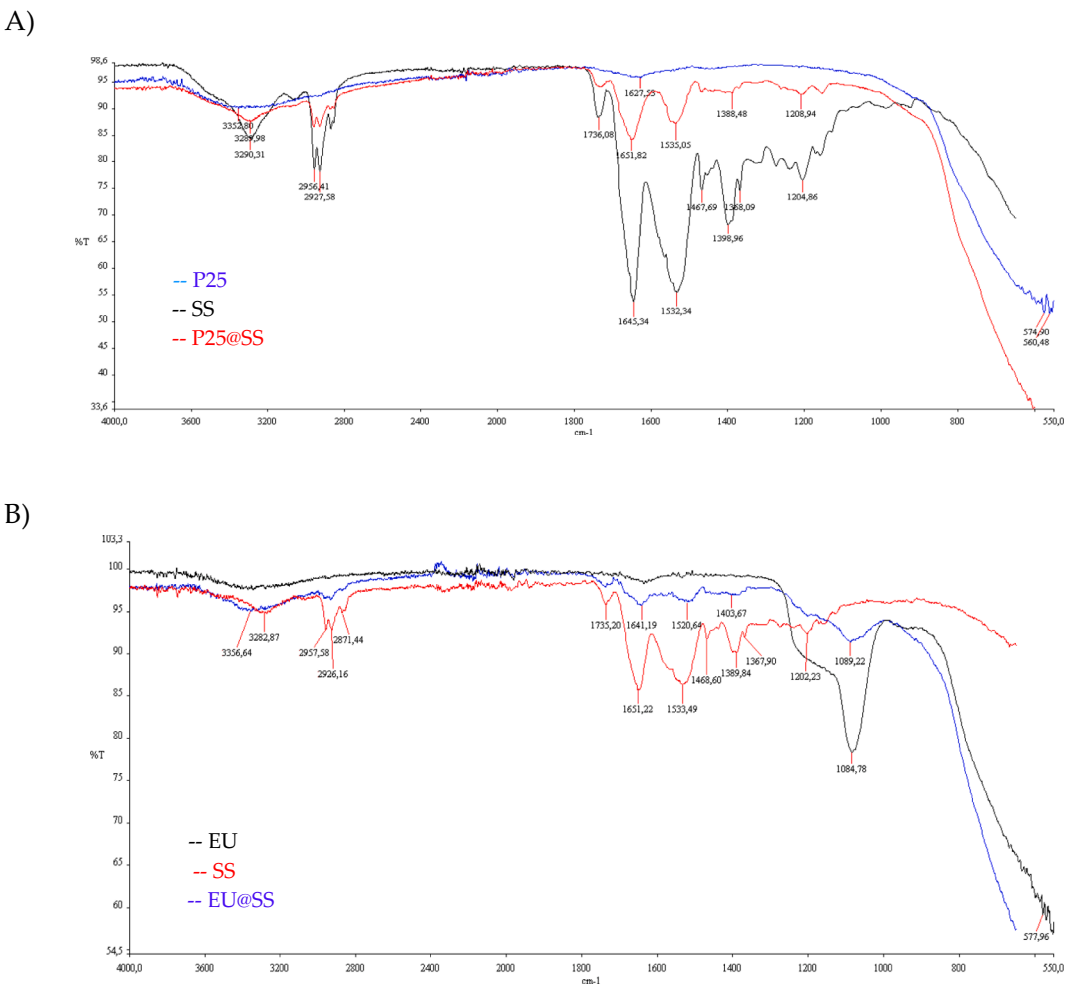

Fig. 4. FTIR-ATR spectra of dried sample, comparing starting materials with A) P25@SS and B) EU@SS samples in the range of 550–4000 cm^{-1}.

Overlap with the starting materials for the EU@SS product is shown in Fig. 4B. The spectrum of EU (black line) is mainly characterized by the peak at 1084 cm^{-1} ascribable to Si—O—Si stretching since EU is commercially described as SiO_2 coated TiO_2, while the band at 577 cm^{-1} is representative of TiO_2 matrix. EU also exhibits an additional band at around 950 cm^{-1} for stretching of Si—O— species of Si—O—Ti [37]. Differing from P25, the broad band at about 3350 cm^{-1} for the O—H stretches is less marked, reduced by interaction with the silica shell.

In the EU@SS spectrum (blue line in Fig. 4B), there is a significant decrease in the Si—O—Si signal at 1084 cm^{-1} (characteristic of precoating), suggesting a transition to a new type of external coating. In fact, characteristic peaks of SS are observable, though they are slightly shifted toward lower frequencies, such as 1641 cm^{-1} and 1520 cm^{-1}, along with the disappearance of the peak at 1389 cm^{-1} which is attributable to C—H stretching.

3.1.3. X-ray diffraction

X-ray diffraction analysis was performed to confirm that the crystalline structure of P25 TiO_2 nanoparticles did not change when mixed with SS, in the composite P25@SS sample. As shown in Fig. 5, the XRD

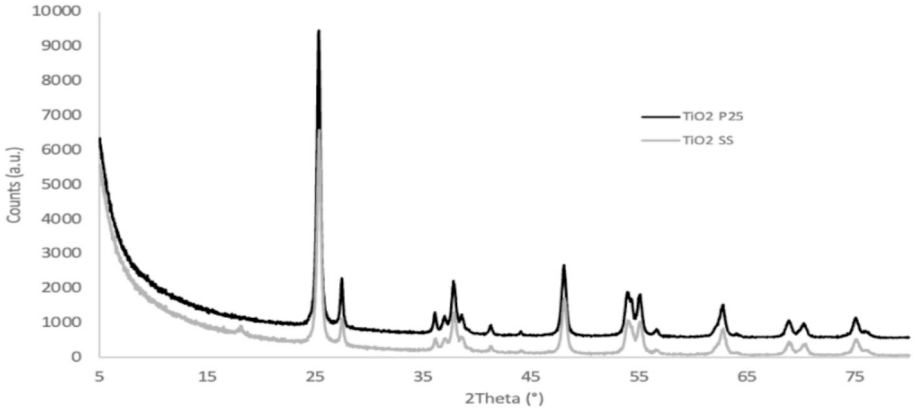

Fig. 5. XRD pattern of P25 and P25@SS nanoparticles.

patterns of pristine and composite TiO_2 NPs are overlapping, revealing a biphasic composition, consistent with the known structure of P25, which comprises approximately 80 % anatase and 20 % rutile phases. Fig. 5 shows that the most intense diffraction peak appears at 25.3° (2θ), corresponding to the (1 0 1) plane of the anatase phase, while additional reflections at 27.4° (rutile 1 1 0) and 36.1° (rutile 1 0 1) confirm the presence of rutile. Further characteristic peaks at 37.8° (anatase 0 0 4), 41.2° (anatase 1 1 2), and 54.3° (anatase 105/rutile 211) reinforce the identification of a mixed-phase TiO_2 structure, in line with established literature. The sharp and well-defined diffraction peaks indicate the high crystallinity of the sample, validating the selection of P25 as a suitable UV-active reference material for surface modification studies. In addition to the TiO_2 phases, a minor peak observed at 61.3° (2θ) corresponds to the Ti_2O_3 sub-oxide, which is known to adopt a rhombohedral crystal structure, unlike anatase and rutile TiO_2, which both exhibit a tetragonal structure. The presence of this sub-oxide phase, although minor, may reflect trace-level non-stoichiometry or surface defects in the commercial P25 batch. These crystallographic insights provide a critical structural baseline for evaluating potential changes induced by functionalization with sodium surfactin and for understanding their impact on the photocatalytic and photostability profiles of the modified material.

3.1.4. Particle morphology: SEM, TEM

The surface morphology of the selected SS-modified sample, abbreviated with P25@SS and EU@SS, is shown in Fig. 6. SEM images of heterocoagulated composites are different from those of pristine TiO_2 or TiO_2 + SS physical mixtures.

In particular, P25 exhibited the typical granular and irregular morphology of uncoated TiO_2, while EU showed more compact and smoother aggregates, likely due to its commercial surface treatment. Upon surface functionalization with SS, both materials displayed a more homogeneous coating layer, with smoother textures and reduced surface roughness, suggesting effective ligand interaction. In contrast, physical mixtures retained a clear phase separation between TiO_2 particles and the flake-like aggregates of surfactin, indicating the absence of surface association, while the morphology of pure SS was characterized by large, amorphous, lamellar structures.

The TEM images of the investigated titanium dioxide powders are shown in Fig. 7. We investigated the samples subjected to the normal process of resin inclusion (A and C) and avoiding it (B and D). As previously observed, P25 NPs exhibit spheroidal morphology, well-defined, electron-dense nanoparticles with typical primary particle diameters of 20–30 nm [38], and moderate aggregation. The P25@SS composite displayed better dispersion with poorly defined nanostructures. The TEM images of P25@SS confirmed that the TiO_2 nanoparticles were almost embedded in the SS matrix, in agreement with the successful heterocoagulation process and indicating successful surface interaction. However, to rule out the influence of the resin used in sample preparation, we compared the samples prepared with and without resin,

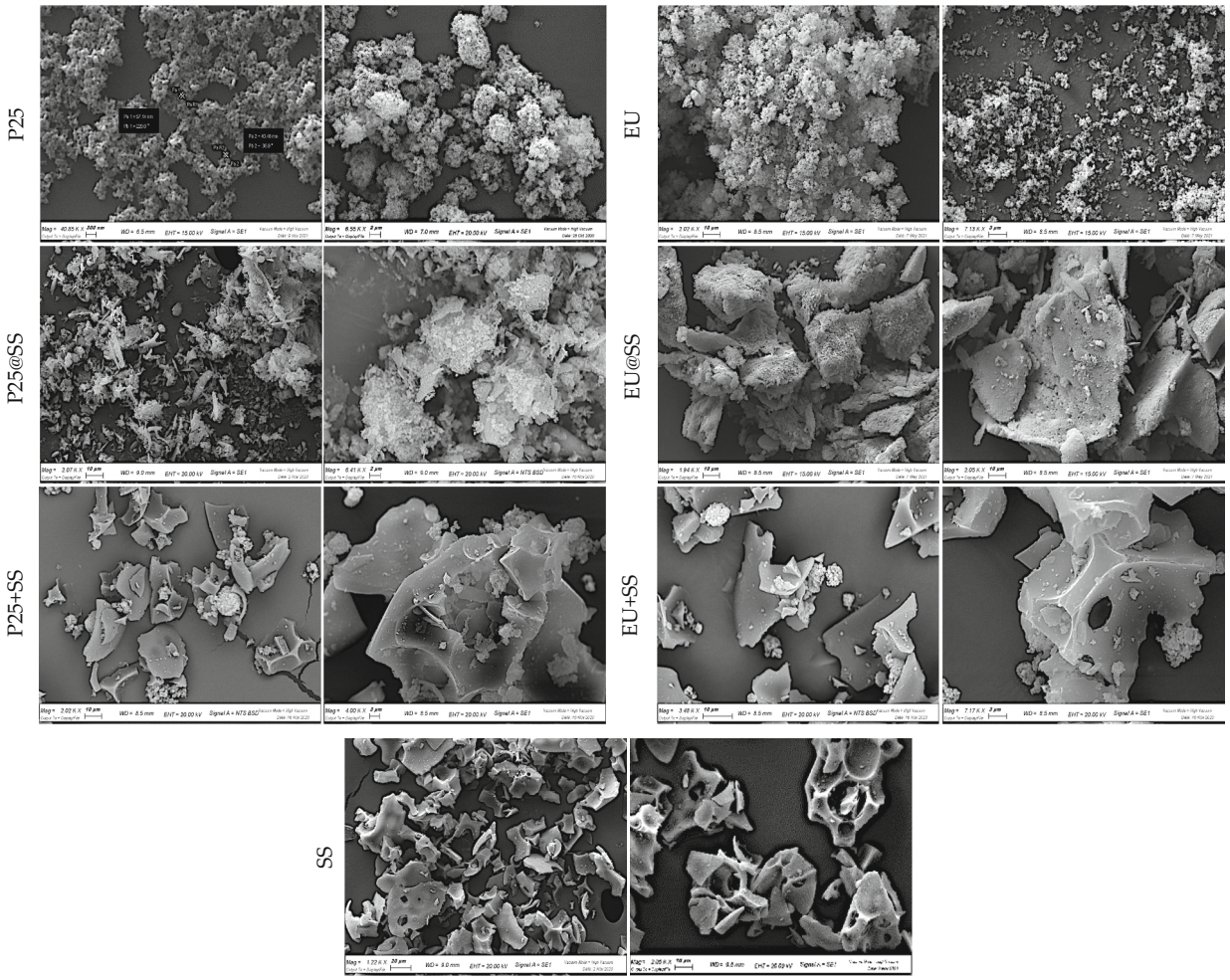

Fig. 6. SEM images of the starting materials and SS-modified TiO_2 (in comparison with the physical mixture of EU + SS or P25 + SS) morphologies at different magnifications (Mag). The SEM-EDS analysis is reported in Fig. S4.

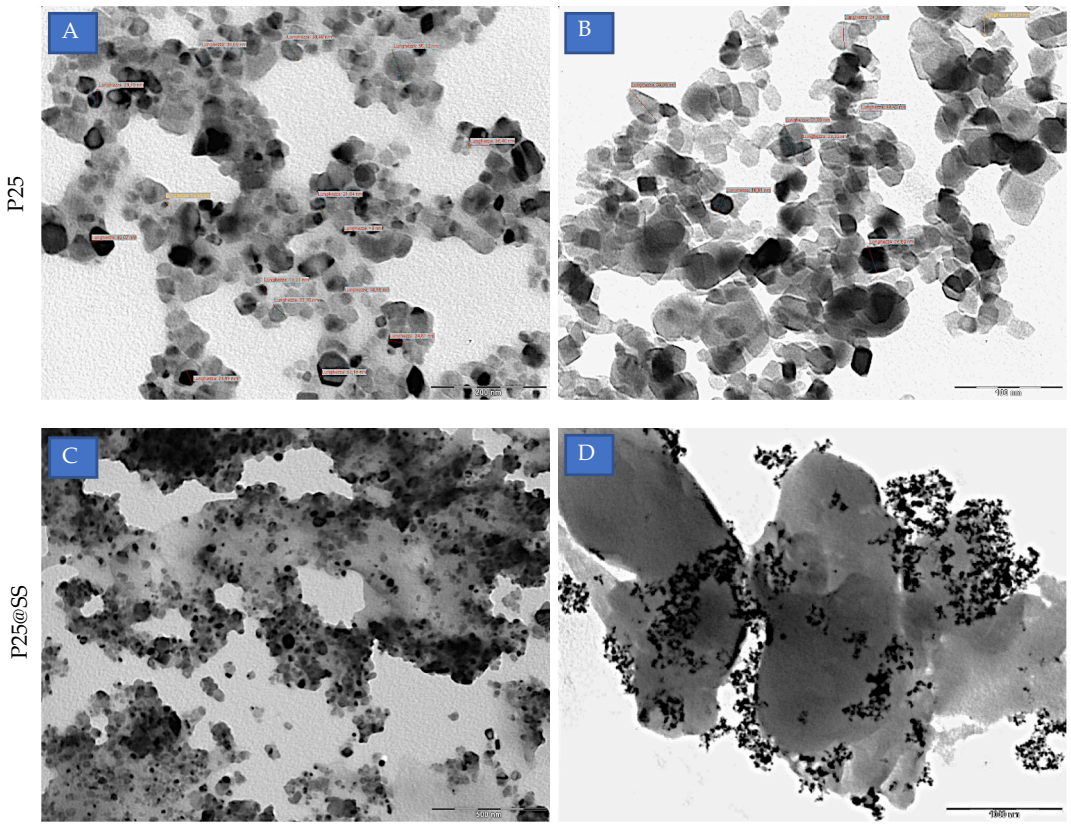

Fig. 7. TEM measurement of TiO_2-based samples on a copper grid with resin inclusions (A and C) and without inclusion in resin (B and D).

which proved to be fundamental for keeping the particles well separated in the case of the P25@SS sample. These results suggest the formation of an interfacial layer in functionalized systems and highlight differences in coating morphology between pristine TiO_2 and P25@SS.

3.2. TGA/DSC measurements

In order to achieve a direct quantification of the organic surfactant content on the TiO_2 surface, thermal analysis was performed for both the pristine materials and optimized SS-modified samples (Fig. 8).

The weight losses (%) detected at 900 °C by TGA are shown in Fig. 8A, calculated as the difference between the sample weights before and after the heating process. Regarding P25, the minimal weight loss observed was due to the evaporation of water (0.91 %). This was slightly higher for EU because it is a commercial product with a SiO_2 coating and an expected higher concentration of adsorbed water. In contrast, the

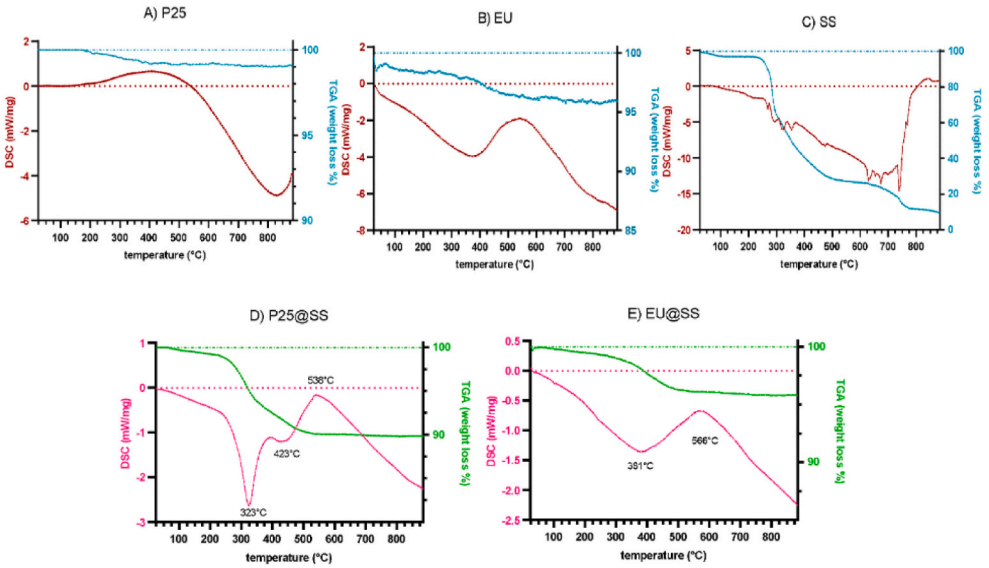

Fig. 8. Results of TGA coupled with the DSC for both pristine materials and optimized SS-modified samples. Weight loss (%) was detected at 900 °C in Fig. 7A; TGA measurements (Bordeaux line) and DSC curves (cerulean-blue line, Endo-Down) were performed at a heating rate of 10 °C/min temperature range of 24–900 °C in Fig. 7B. (For interpretation of the references to color in this figure legend, the reader is referred to the web version of this article.)

thermal behavior of the organic molecule (SS) alone was characterized by significant biosurfactant decomposition, up to a weight loss of 90.55 %. In the SS-modified samples, the difference in TGA mass loss compared to the respective pristine materials is attributed to the amount of SS adsorbed (approximately 10 wt%), which is in agreement with the estimated amount needed to stabilize the P25 sample (13,2 wt%). Otherwise, the weight loss observed in the EU@SS sample (approximately 4 %) suggests that the chosen EU@SS (1:1) sample, containing 100 % of the SS content relative to EU, indicates that this sample has an excess of SS that is not adsorbed on the surface.

Furthermore, the analysis of materials using the DSC technique was conducted to directly assess the transition temperatures of the samples in their natural state, illustrating the change in enthalpy as a function of temperature (Fig. 8B). By integrating these two techniques, it was possible to ascertain the physicochemical transformation of the sample and its corresponding temperature.

The DSC curves of P25 are characterized by an exothermic peak with a Tm of 414 °C, which is attributed to the phase transformation from anatase to rutile, in agreement with the literature [39]. The maximum peak temperature (Tm) of a broad melt is the most significant and it is therefore used to distinguish different TiO_2 NPs forms.

Regarding EU, the higher decrease in weight than P25 can be attributed to the increased desorption of physisorbed water, as confirmed by the corresponding endothermic peak on DSC. This assumption is motivated by the fact that SS is a hygroscopic material; there, it can absorb water from its surroundings during handling.

The thermogram of P25@SS showed significant differences compared with P25 ones. The main characteristics that differentiate the peaks are (i) peak area proportional to process enthalpy, (ii) peak direction (endothermic or exothermic process), and (iii) shape (defined by onset, peak temperature, end point, and inflection), all of which depend on the quality of the surface coating analyzed [40]. After the first stage of dehydration (at temperatures below 100 °C), the thermal treatment of P25@SS was accompanied by two endothermic peaks (Tm_1 323 °C and Tm_2 423 °C), proportional to a large heat request. The second stage corresponded to the degradation of organic matter (SS) from the sample. The two distinct peaks observed in DSC may be associated with the denaturation of the backbone chain, leading to the release of the entrapped biosurfactant and its thermal decomposition, along with the breakdown of various types of bonds (functionalization and complexation) on the TiO_2 surface. However, the same considerations cannot be carried out by observing the adduct EU@SS. As a result of functionalization, no different thermal profile was observed compared to that of pristine EU. The first thermal domain, characterized by an endothermic peak (Tm_1 381 °C), did not differ significantly from the corresponding peak of TiO_2 EU (Tm_1 373 °C), as well as the temperature of the post-transition baseline at 566 °C, most likely because the excess SS masks the information regarding the processes occurring at the substrate-coating interfaces for EU@SS.

3.3. Photoreactivity (safety test)

The photocatalytic activity of TiO_2-based samples was examined and linked to potential hazards associated with photo-generated reactive oxygen species (ROS) [41]. Therefore, the depletion of a dye (AB9) under visible-light irradiation was investigated using an optimized methodology [42,43]. The dye depletion efficiency of TiO_2 modified samples with and without UV light activation are presented in Table 3. As expected, P25 with an anatase crystalline structure showed the highest depletion efficiency (70.84 %) due to its high photocatalytic reactivity, in addition to the contribution of dye adsorption in the dark, highlighted by a slight discoloration of AB9 (4,76 %). Conversely, EU TiO_2 did not exhibit any photoresponsiveness, confirming that the rutile phase is less active and may also be inhibited by the silica shell. The slight improvement in efficiency shown by the EU@SS sample (1,78 %) is most likely due to the increase in EU dispersion in the presence of SS

Table 3
AB9 dye depletion expressed as percentage of dye depleted vs the initial concentration (Depletion efficiency %) at "dark" or "UV" conditions.

Sample	Condition of analysis	Dye depletion efficiency (%)	±SD
AB9	Dark	0	Nd
	UV	**0**	**Nd**
P25	Dark	4,76	0,78
	UV	**70,84**	**0,09**
EU	Dark	0,26	0,03
	UV	**0,64**	**0,00**
SS	Dark	0,04	0,46
	UV	**0,1**	**0,03**
P25 + SS (mix)	Dark	0,33	0,08
	UV	**17,35**	**0,76**
P25@SS (13,2 wt%) ultrapure water	Dark	0,54	0,06
	UV	**0,7**	**0,06**
P25@SS (1:1) ultrapure water	Dark	0,82	0,09
	UV	**1,19**	**0,61**
SS@P25 (1:1) ultrapure water	Dark	0,47	0,14
	UV	**2,63**	**1,60**
EU@SS (1:1) ultrapure water	Dark	0,12	0,11
	UV	**1,78**	**1,75**

(Table 3) which may increase the number of photoactive surface groups available. None of the TiO_2-SS samples investigated, regardless of the selected design options, exhibited any significant depletion of the AB9 dye, confirming the effective ability of SS, intimately bound to the TiO_2 surface, to suppress photocatalytic activity. However, P25@SS (13,2 wt %) was confirmed to be the best sample in terms of photostability, showing the lowest reactivity. To assess how the intimate interaction between TiO_2 and SS in the heterocoagulated sample influenced the photostability, we also evaluated the reactivity of the physical mixture (P25 + SS Mix, 9:1) and confirmed that, in this case, the SS matrix is not as effective in suppressing the dye depletion efficiency (approximately 17 %).

Two mechanisms of photocatalytic quenching by the SS phase, heterocoagulated onto the TiO_2 surface, may be hypothesized: 1) steric hindrance with consequent electron scavenging phenomena and 2) direct injection of SS electrons on the TiO_2 conduction band, suppressing radical generation by the valence band (Fig. S5) [43,44].

3.4. Dustiness index

The dustiness of a powder is an important physicochemical indicator of worker exposure and contributes to the definition of the human health and safety aspects of the chemical/material production and processing phase (Step 2 of the JRC SSbD framework [45]), particularly relevant for the definition of the SSbD profile of ultrafine powders. The number-based dustiness index (DIRN) and mass-based dustiness index (DIRM), together with preliminary data results of the dustiness index determination, such as the specific surface area and bulk density, are reported in Table 4. By comparing the samples in terms of BET, there were no significant differences. The only parameter that exhibited a discernible difference was the bulk density, with P25 showing the lowest density due to the presence of many aggregates and resulting inter-particle voids. In terms of the Dustiness Index, a comparison between P25@SS and pristine P25 showed a restricted range of values, without significant improvement. Thus, even if dustiness reduction was not the goal of the SSbD strategy implementation, the functionalization with SS did not lead to an increase in the emission potential despite the greater dispersibility of TiO_2 in the SS matrix.

3.5. Ecotoxicity

The materials were characterized, their behavior was analyzed in freshwater as a test medium, and their toxicity was assessed by performing an algae assay and ZET test.

Table 4
Results obtained from Vortex shaker - Respirable fraction (<4 μm).

Material name					Specific surface area (m^2/g)	Bulk density		Median	Mode 1
	(mg/kg)	CV (%)	(#/mg)	CV (%)		(g/cm^3)	CV (%)	(μm)	(μm)
P25	6.16E+03	3.01E+01	1.03E+05	3.04E+01	4.87E+01	1.64E-01	4.81E+00	1.17E+00	1.84E+00
P25@SS	2.46E+03	5.24E+01	2.00E+05	3.32E+01	4.46E+01	4.05E-01	5.24E+00	8.10E-01	1.84E+00
EU	1.04E+05	3.52E+01	1.28E+06	6.88E+00	4.95E+01	9.37E-02	6.49E+00	8.70E-01	1.16E+00

3.5.1. Preliminary algae assay

Primarily, the algae assay is a preliminary test to determine the acceptability or non-acceptability of nanoparticles in the specific context of use and regulatory standards. This is a growth inhibition test for aquatic algae and cyanobacteria. To assess whether this value is acceptable, it is typically compared to the regulatory thresholds or guidelines set by relevant authorities. These thresholds can vary depending on the jurisdiction and specific applications of a substance. For example, some regulatory bodies may have established permissible limits for the ecotoxicity of substances in water bodies and other environmental compartments. Furthermore, it is essential to consider a broader context, including the potential for bioaccumulation and its long-term effects on ecosystems. Engaging with experts in ecotoxicology or regulatory affairs can also be beneficial for thorough evaluation.

In this study, we determined the concentration of particles that may be toxic to algae. The objective of this test was to screen for toxicity in different samples. However, additional assessments are necessary to ascertain more specific effects. Detailed data obtained to determine the acceptability of the materials are summarized in Table 5.

It is evident that surface modification by the biomolecule of the titanium nanoparticle facilitates a reduction in the ecotoxic effect it has on algae. In this instance, the functionalization of the nanoparticles increased the EC50 from 1.4 to 18 mg/L by a factor of ten (10 times more). This incorporation of biomolecules represents a promising alternative for reducing the ecotoxicity of the nanoparticle.

EC50 is a commonly used measure in ecotoxicology to quantify the concentration of a substance that causes a specified effect in 50 % of a test population within a specified time period. In the context of ecotoxicity studies of titanium nanoparticles on algae, EC50 represents the concentration of titanium nanoparticles that leads to a 50 % reduction in the growth or viability of the algae population being studied. Consequently, the lower the concentration, the more toxic the nanoparticles are, as evidenced by the fact that a lower concentration is required to reduce algal growth to 50 %. Conversely, increasing this concentration reduces the toxicity of the nanoparticles. It is very important to underline that the result obtained is based on the adsorbed amount of SS of only 13,2 wt% on TiO_2. It should be noted that this type of test cannot measure other effects, such as chronic effects, and is therefore only capable of measuring the effects on growth or viability.

3.5.2. Acute fish embryotoxicity assay (AFE)

The NPs presented a higher degree of aggregation in freshwater than in ultrapure water. Interestingly, the dispersion after 24 h was more homogeneous (<PI) and the size of the aggregates was smaller in the later. However, the dispersion in freshwater was less homogeneous after 24 h of incubation, and the NPs formed larger aggregates (Table S2).

Table 5
Preliminary algae assay results. The data in the table express parts per million (ppm) or mg/L of particles in the aquatic environment. EC50 represents the concentration of titanium nanoparticles that leads to a 50 % reduction in the growth or viability of the algae population being studied.

Sample	EC50 algae	95 % interval
P25	1.45305	1.010; 6.070
SS	24.9888	10; Inf
P25@SS	18.0632	10.282;72.766

P25@SS did not exert acute toxicity in zebrafish embryos (lethal or sublethal effects at the endpoints measured in our test). It is worth mentioning that some sublethal parameters could only be registered until a maximum concentration of 10 mg/L; at the highest concentration (100 mg/L), embryos were entirely covered by a layer of NPs that did not allow observation of the embryos under the microscope.

Finally, we tested the biomolecule alone up to the maximum concentration expected in 100 mg/L of TiO_2 NPs (13,2 mg/L), and it seems that the biomolecule alone can produce some sub-lethal effects (Fig. S6, A). Further studies are required to understand the toxic effect of the biomolecule alone.

Unmodified P25 did not display acute toxicity to zebrafish embryos either (Fig. S6, H and J); we can conclude that functionalization does not increase toxicity. In view of the results from the ecotoxicological test, no potential acute toxic effects in freshwater were observed for SS-modified titanium dioxide in aquatic organisms (Tables S3-S5).

3.6. Preliminary in vitro evaluation: cell viability assay in BEAS-2B, RAW264.7, and HSF cell lines

A preliminary evaluation of the in vitro cytotoxicity of P25, SS, and P25@SS was conducted using the BEAS-2B, RAW264.7, and HSF cell lines. Cells were exposed to concentrations ranging from 1 to 200 μg/mL for 24 h.

Cell proliferation results in BEAS-2B human bronchial epithelial cells of powders are shown in Fig. 9. The starting materials (P25 and SS) were used as controls for comparison. As reported by previous studies [46], TiO_2 NPs did not cause any cytotoxicity in lung epithelial cells at concentrations below 10 μg/mL for longer exposure times. However, at higher concentrations, a toxic effect was reported at 6 h, which disappeared after 24 h. However, a significant reduction in cytotoxicity was observed in cultures exposed to P25@SS under the same critical concentration/exposure conditions for pristine P25. Notably, a slight increase in BEAS-2B cell viability was reported after 6 h-treatment with P25@SS particles at 1 and 10 μg/mL.

SS was found to exert dose-dependent cytotoxicity in BEAS-2B cells. For 6 h of treatment, 1 μg/mL and 10 μg/mL of native SS did not exhibit any cytotoxicity, but concentrations of 100–200 μg/mL cause a decrease in cell viability, similar to the positive control. A mirror-like situation is seen after 24 h for the higher concentrations, but surprisingly the concentrations below 1.0 μg/mL even lead to an increase in cell viability, which is typically observed in nanomaterial viability tests. However, although toxicity values at 100 and 200 μg/mL represent significant experimental evidence, these are circumstances that differ greatly from the actual concentrations used. Indeed, in the functionalization product in which the wt ratio of SS is reduced (about 10 %), the same trend is not recorded.

Furthermore, Fig. 9 shows the cytotoxicity data of powders determined by performing the WST-8 assay on the mouse alveolar macrophage cell line RAW264.7. The macrophage cell RAW264.7 has long been used as an in vitro model to study the response of inflammatory molecules to various synthetic stimuli. Macrophages are the first cells of the immune response and represent the innate immune system; their response is crucial for the survival of cells, tissues, organs, and systems [47]. Therefore, from the perspective of the possible risk of inhalation of NPs, the effects of dust on immunomodulator viability were assessed based on the dose and exposure times. By continuing to investigate from

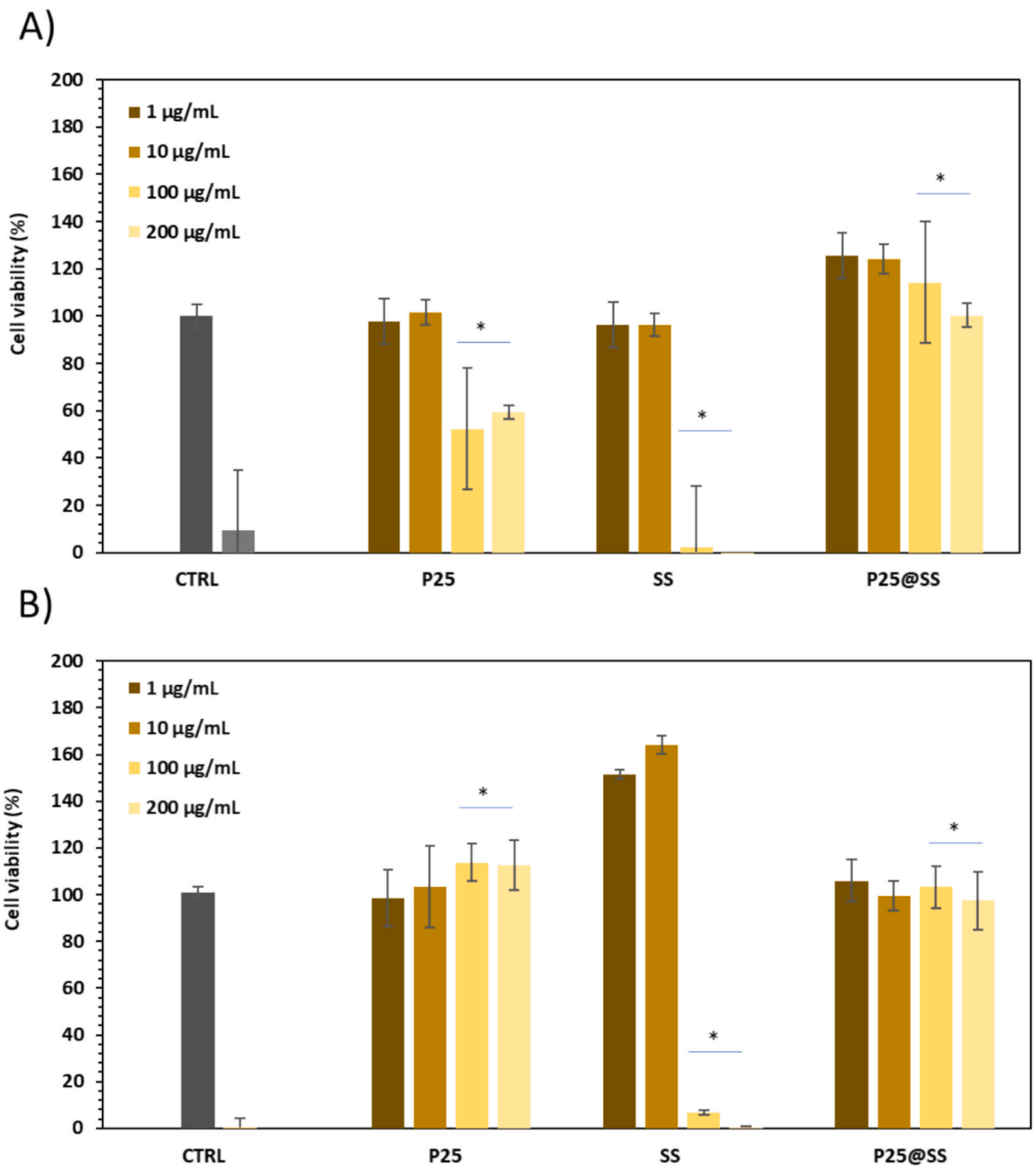

Fig. 9. Cell proliferation results of BEAS-2B cells treated with increasing concentrations of particles for A) 6 h, B) 24 h. Dark gray bar shows negative control and as positive control, 10 % DMSO was used as indicated as light gray. Asterisks indicate significant differences between the negative control vs P25, control vs. SS, control vs. P25@SS, SS vs. P25@SS, and P25 vs. P25@SS for 100 and 200 µm/mL.

the perspective of the inhalation risk of NPs, the effect of powders as such or surface-functionalized powders on the viability of RAW264.7 cells must be analyzed to assess their nanosafety. As illustrated in Fig. 10, the viability of RAW264.7 cells decreased abruptly at P25@SS concentrations of 100 and 200 µg/mL both after 6 and 24 h, compared to the control. At lower concentrations, cytotoxicity was less marked but remained greater than with TiO_2 naked. However, this evidence can be substantiated by observing the cytotoxicity data of macrophages exposed to SS. In fact, with reference to SS treatment alone, the cell viability of inflammatory cells recorded the lowest value with increasing concentrations from 100 µg/mL. Similar to what was observed in BEAS-2B cells, SS at lower concentrations (1 and 10 µg/mL) had the greatest beneficial impact on cell viability.

A study of the intracellular molecular and genetic mechanisms induced by SS is essential for elucidating the effects of surface-functionalized TiO_2 on the viability of these cell lines. Finally, examining the data collected from the pristine P25 treatment, no difference was observed in the concentration-dependent effects in RAW264.7 cell viability at either time point of exposure, except for a favourable effect at 200 µg/mL after 24 h.

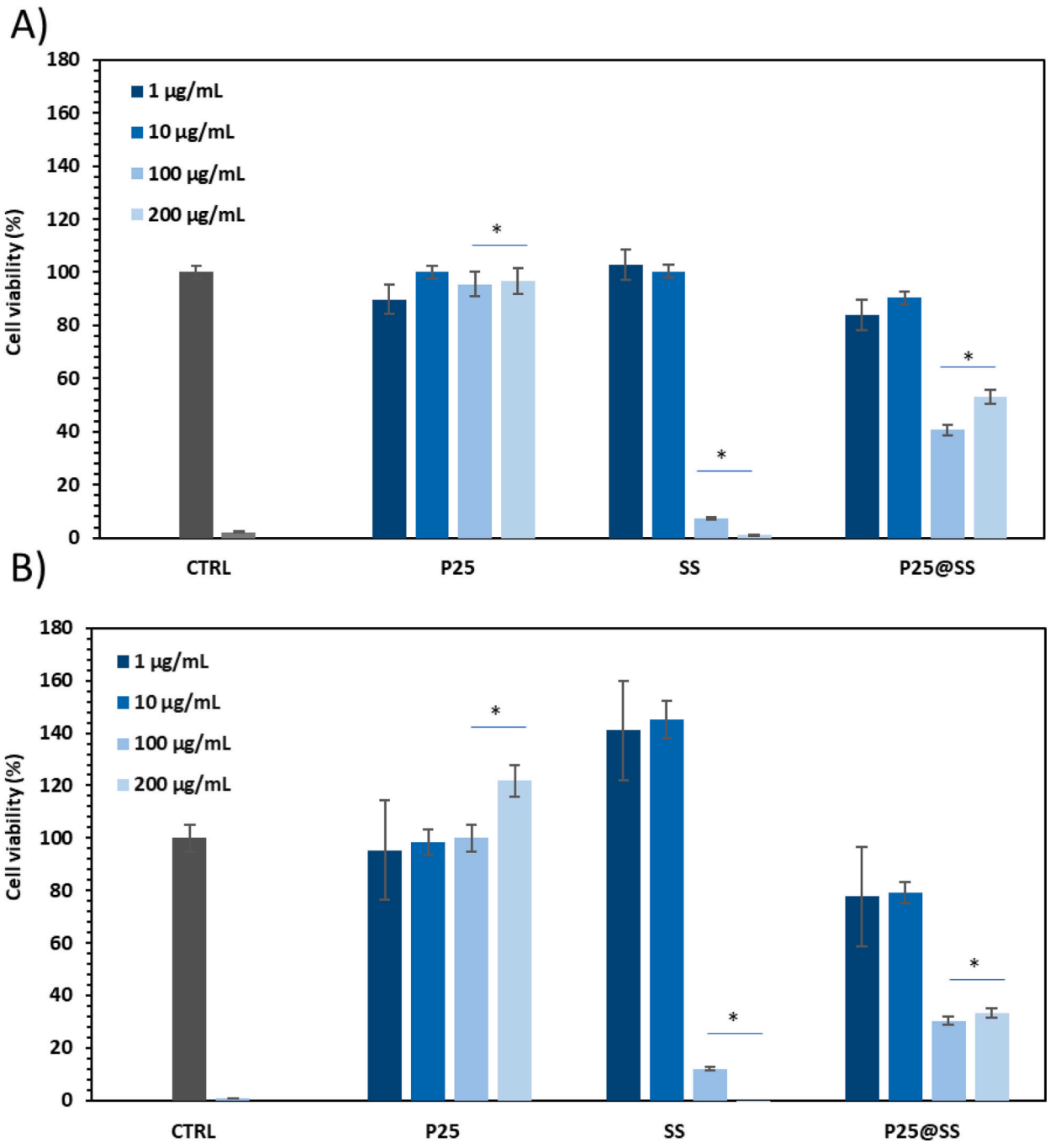

Fig. 10. Cell proliferation results of RAW264.7 cells treated with increasing concentrations of particles for A) 6 h, B) 24 h. Dark gray bar shows negative control and as positive control, 10 % DMSO was used as indicated as light gray. Asterisks indicate significant differences between the negative control vs. SS, control vs. P25@SS, P25 vs. P25@SS for 100 and 200 µg/mL.

The preliminary cytotoxicity results of HSF treated with varying concentrations NPs provided important insights into concentration-dependent effects. As seen in Fig. 11, at the lowest concentration (1 µg/mL), all treatments (P25, SS, and P25@SS) maintained or slightly enhanced cell viability compared to the negative control (NC), indicating no cytotoxic effects at this concentration. As the concentration increased to 10 µg/mL and 100 µg/mL, cell viability consistently remained above 100 %, particularly in P25 and P25@SS treatments, demonstrating a dose-independent response within this range. This suggests that these substances, even at higher concentrations, are well tolerated by fibroblast cells, without causing any significant reduction in viability. At the highest concentration (200 µg/mL), there was no marked decrease in cell viability, indicating that both P25 and SS, either individually or in combination, exhibit strong biocompatibility even at elevated doses. Interestingly, the composite P25@SS did not introduce any additional cytotoxic effects compared to P25 or SS alone, suggesting that the combined formulation is as safe as the individual components. These findings highlight that the concentration range tested (1–200 µg/mL) does not negatively impact fibroblast cell viability, making these substances highly suitable for use in topical applications such as sunscreens, where high concentrations of active ingredients are often required for effective UV protection. The concentration-independent viability across all treatments further emphasizes their potential for safe and long-term use in skincare formulations.

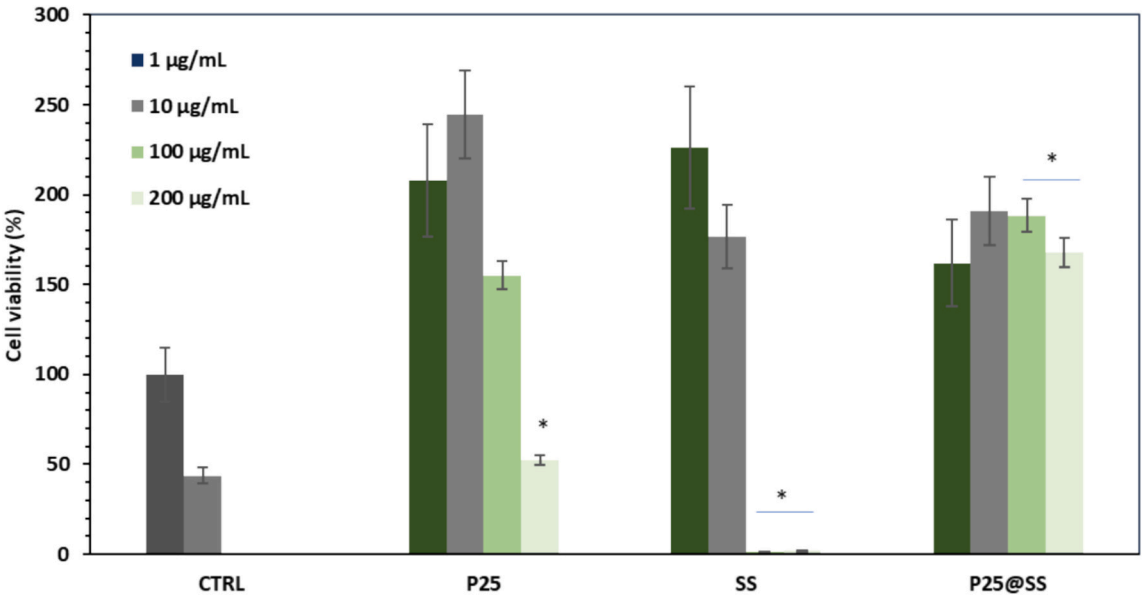

Fig. 11. Cell proliferation results of HSF cells treated with increasing concentrations of particles for 24 h. Asterisks indicate significant differences between the negative control vs P25 for 200 µg/mL, control vs. SS, SS vs. P25@SS SS for 100 and 200 µg/mL, and P25 vs. P25@SS for 200 µg/mL.

3.7. Photoprotective efficacy

By means of spectrophotometric measures, the amount of UV radiation (calculated from transmittance) passing through the film was evaluated on the set of O/W formulations. Photostability studies were carried out with a solar simulator device and in vitro SPF analysis was performed according to ISO 24443:2012.

It was observed that all the formulations tested turned out to be photostable and UV filtering parameters are shown in Table 6.

In the analysis of the base emulsion (Formula A) and the emulsion containing solely the specified quantity of the SS ligand (Formula C), the data do not demonstrate statistical significance. However, they are presented to substantiate the complete absence of UV filtering capabilities in the formulation's constituents and Sodium Surfactin. Notably, both formulations exhibit a negligible SPF value, approximately 1. Of particular interest is the pattern observed when comparing formulations incorporating P25 (Formula B) and P25@SS (Formula D). Both formulations exhibit reduced absorption in the UVA region of the spectrum, yet they demonstrate a satisfactory SPF value relative to the percentage of UV filters employed (approximately 10 %), in comparison to the maximum permissible amount of 25 % as stipulated by European regulation 1223/2009. The attenuation of UVB by TiO_2 is primarily attributed to absorption, necessitating the minimization of particle size to enhance SPF (thereby increasing the specific surface area exposed to incident radiation), and consequently, UVB protection, while achieving a desirable appearance due to its transparency [48,49]. To optimize UVA protection, however, the TiO_2 particle size should not be excessively small, as its scattering activity significantly contributes to shielding in this spectral region; this activity diminishes with decreasing TiO2 size.

As for P25@SS, Formula D shows an increase in terms of SPF (8.52) compared with P25-based Formula (SPF of 6.45). This result, totally unattended, suggests that the "safe by design" functionalization does not adversely affect the UV filtration parameters, and, on the contrary, allows a slight increase in them. Thus, it is inferred that the coating of TiO2 particles introduces a variable in the optimal dispersion of the UV filter, increasing its effectiveness.

Differences are also becoming evident in the value of λ Critical. Sunscreen products that primarily offer UVB protection typically have a critical wavelength of less than 320 nm, whereas those providing both UVB and UVA protection exhibit critical wavelengths ranging from 320 to 400 nm [50]. In this study, both Formula B and D meet the requirement of a λ Critical value greater than 370 nm, as necessitated for sunscreens.

Similarly, to the λ Critical, SPF label/UVAPF ratio provides an evaluation of the amplitude of the protection across the UV spectra without considering the amount of the filtering activity. Values near to 1 are indicative of a broad-spectrum activity. EC 647/2006 suggests that all solar products have a critical lambda value greater than 370 nm and a UVAPF value of at least 1/3 of the SPF value [48].

Table 6
UV filtering parameters from in vitro SPF analysis of each formulation.

Formulation	Description	SPF	UVA-PF	SPF label	SPF label/ UVAPF	λ critical (nm)
Formula A	Emulsion Base	1.05	Nd	6	Nd	291
Formula B	Emulsion with P25	6.45	2.79	6	2.15	375
Formula C	Emulsion with SS	1.01	Nd	6	Nd	290
Formula D	Emulsion with P25@SS	8.52	2.75	6	2.19	374

4. Discussion

In the present paper, the structural design, development, physicochemical and biological characteristics of biosurfactant-stabilized TiO_2 nanoparticles leading to effective biocompatible UV filters were discussed. Specifically, this research examined the efficacy of a novel Safe and Sustainable by Design approach on nanoTiO_2 to mitigate the side effects of the inorganic filters, such as their photo reactivity. It was determined that the fate and behavior of individual and aggregated TiO_2 NPs in the presence of environmental compounds are primarily governed by the complex interplay between electrostatic attractive and repulsive interactions, steric and van der Waals interactions. Consequently, we have successfully stabilized TiO_2 NPs against aggregation, sedimentation, and other destabilization phenomena by employing a lipopeptide (Sodium Surfactin, SS), a biosurfactant molecule obtained through fermentation, as a "capping agent". Utilizing a method of self-assembly by heterocoagulation, we reported the functionalization with

SS of two different types of titanium dioxide nanosized particles (P25 and EU).

The use of P25 was a deliberate and scientifically grounded choice, as its high photoreactivity, attributable to its predominant anatase content, makes it a stringent and widely recognized benchmark for evaluating surface functionalization strategies aimed at reducing photocatalytic activity. In addition, its broad industrial relevance and frequent application as a reference material in nanotoxicology and materials science underscore its suitability as a representative model for the development of widely applicable safety enhancements. On the other hand, Eusolex T-Avo was selected as a benchmark due to its commercial relevance as a surface-treated TiO_2, allowing us to compare the performance of SS functionalization against an industry-standardized formulation.

Through a meticulous evaluation of the synthesis parameters to obtain TiO_2 + SS-based composite, we assessed the efficiency of the colloidal approach by modifying the sequence of reagent addition, synthesis conditions, solvent, sonication, and optimal ratio of species involved.

Subsequently, the colloidal properties, specifically the particle size distribution as determined by dynamic light scattering (DLS) and the zeta potential as measured by electrophoretic light scattering (ELS), were correlated with various parameters through a multi-technical approach. This approach included morphology analysis using scanning electron microscopy (SEM) and transmission electron microscopy (TEM), along with energy-dispersive X-ray analysis (EDX) for surface chemistry, Fourier-transform infrared spectroscopy (FT-IR), and thermal analysis via thermogravimetric analysis (TGA) and differential scanning calorimetry (DSC). This comprehensive analysis facilitated the development of an optimized prototype for further investigation, designated as P25@SS 13,2 wt%. As previously mentioned, electrostatic interactions are the primary mechanism underlying the formation of these products, and this was examined through zeta potential measurements.

In this regard, the main driving force was observed in the P25@SS sample, obtained through an electrostatic interaction between negatively charged SS and positively charged titania nanoparticles, facilitated by mixing the sols in well-defined ratios, and reacted under magnetic stirring for 24 h. The optimized prototype of P25@SS was obtained by dispersing 13,2 wt% of SS in UW compared to P25, exhibiting a ζ-potELS value of −24.8 mV, pH i.e.p. of 4.3, and dDLS of 315 ± 8 nm (PdI 0.4). As demonstrated by hydrodynamic diameter (dDLS) and zeta potential measurements, the coating stabilized the colloidal behavior of titania in aqueous suspension, resulting in a reduction in dimensional size compared to pristine P25 (599 ± 50 nm and PdI 0.5), and a different surface reactivity (ζ-potELS of P25 is +41.1 mV with a pH i.e.p. of 6.13). Considering the presence of an electrostatic interaction between the particle surface and SS, and the DLS data, one or more layers of SS on the particle surface can occur depending on the added SS concentration. Thus, it is safe to assume that SS forms a layer on the particle surface.

Morphologically, the unmodified nanoparticles of P25 were observed by SEM as being spherical in shape undergoing a structural variation following functionalization, which was better elucidated by TEM. TGA analysis of pristine starting materials and modified TiO_2 NPs, conducted in the 24–900 °C temperature range, air/N_2 mixture (40 mL/min air and 80 mL/min N_2) at a heating rate of 5 °C/min, was performed to estimate the NPs surface coverage rate for each ligand. The TGA of pristine P25 did not exhibit any mass loss in the temperature range investigated, confirming the purity of the starting material previously observed by FT-IR analysis. Regarding functionalized P25 NPs, a mass loss of approximately 10 % was observed for P25 NPs functionalized with SS ligands, but only a minimal amount was observed for EU@SS compared to pristine EU. Furthermore, DSC analysis corroborated the chemisorption of the SS ligands on P25, demonstrating that endothermic processes occurred from approximately 300 to 500 °C, associated with the decomposition of the attached organic fraction. In addition to the comprehensive discussion on the characterization and SS loading amount, the photostability and toxicity issues of these composites have been extensively addressed.

To validate the SSbD approach, the side effects of TiO_2 NPs in terms of photo reactivity were investigated acellularly (Blue Acid 9 assay) as a preliminary photo reactivity evaluation. The photodegradation pattern of Blue Acid 9 under visible light irradiation highlights the highest dye depletion efficiency (70.84 %) for P25 with anatase crystalline structures compared to P25@SS (0.70 %). The ability of SS to act as a detoxifying agent was evident by assuming a dual mechanism of electron scavenging and reduced ROS formation. The results demonstrate that the prepared P25@SS not only significantly mitigates the negative reactivity of P25, thereby reducing its toxicity, but also confirms the efficacy of the coating process when compared to a simple physical mixture (characterized by a dye depletion efficiency of approximately 17.35 % after UV irradiation). Subsequent preliminary in vitro assessment investigated the toxicity of both pristine and modified samples on human and environmental health.

Considering that human exposure to TiO_2 NPs can occur through ingestion, dermal absorption, or inhalation, during both the manufacturing process and their use in products; the propensity for dustiness as powders and the biocompatibility of the nanocomposite with RAW264.7, BEAS-2B, and HSF cells were studied. Firstly, the dustiness indices of the prototype P25@SS and P25 in comparison with the commercial EU were examined to evaluate the safe by design approach from the perspective of impact on workers and/or environmental exposure. The results obtained by the Vortex shaker method revealed no significant differences between the starting material and the coated product, while excluding an increase in emission potential, despite the greater dispersibility of the nanometric titanium dioxide.

In terms of biological interactions, the preliminary biocompatibility assessment of the pristine raw materials and the nanocomposite stabilized by 13,2 wt% SS was performed in three different cell lines. Overall, cell viability data (WST-8 assay) of BEAS-2B and RAW264.7, cells treated with NPs for 24 h, revealed a similar trend. P25 and SS showed dose-dependent cytotoxicity after 6 h of treatment at high concentration (100–200 μg/mL), with a decrease after 24 h, whereas concentrations below 10 μg/mL were not cytotoxic. Of particular interest was the significant reduction in cytotoxicity observed in cultures exposed to P25@SS under the same critical concentration/exposure conditions for uncontaminated P25. Furthermore, cell proliferation results (alamar blue assay) of HSF cells treated with increasing concentrations of particles (1–200 μg/mL) for 24 h excludes the negative impact on fibroblast cell viability, making these substances very suitable for use in topical applications, for safe and long-term use in cosmetic formulations.

In vitro assessments of ecotoxicity were conducted using both an algae test and a zebrafish embryo toxicity (ZET) test. The embryotoxicity evaluations on zebrafish, a freshwater species, indicated no acute toxicity for either the pristine P25 or the surface-modified material. In the growth inhibition assays involving algae and aquatic cyanobacteria, it was observed that the surface modification of P25 nanoparticles (NPs) with biomolecules mitigated the ecotoxic effects on algae. Specifically, the integration of biomolecules onto the nanoparticles increased the EC50 from 1.4 to 18 mg/L, representing a tenfold increase, thereby suggesting a promising strategy to reduce nanoparticle ecotoxicity. Subsequently, the proposed Safe and Sustainable by Design (SSbD) approach demonstrated efficacy in modulating the photo reactivity of TiO_2 without compromising its ultraviolet (UV) filtering properties. The evaluation of the Sun Protection Factor (SPF) in accordance with ISO 24443:2012 revealed that heterocoagulation, in terms of enhanced dispersibility and stability of P25, resulted in an increase in SPF from 6.45 to 8.52. Ultimately, these significant advantages of P25@SS (13,2 wt% SS) over conventional TiO_2-based inorganic filters underscore its potential as a “safe and sustainable by design” solution across various applications.

5. Conclusions

The widespread use of P25 TiO_2 nanoparticles in commercial sunscreen formulations can be partly attributed to the lack of clear regulations and standardized control measures. Although some products use surface-coated TiO_2 to mitigate the known phototoxicity associated with the anatase form, there is a notable lack of systematic studies evaluating the effectiveness, safety, and sustainability of these coating strategies. Our study specifically addresses this gap by providing a comprehensive assessment of an alternative, bio-inspired surface functionalization approach using Sodium Surfactin. We present an in-depth physicochemical characterization alongside a multi-technique evaluation of environmental safety, human health risks, and occupational exposure, all within the Safe-and-Sustainable-by-Design (SSbD) framework, ensuring UV protection performance is maintained.

This study demonstrates the potential of integrating lipopeptides as surface modifiers for TiO_2 NPs within a SSbD framework. The modification of TiO_2 NPs with surfactin, in particular the P25@SS (13,2 wt%) form, effectively enhanced colloidal stability and reduced potential toxicity without compromising the functional properties of UV filters. The successful implementation of the SSbD approach highlights its viability as a strategy for designing safer nanomaterials, addressing both environmental and human health concerns associated with the widespread use of ENMs. These findings underscore the importance of early stage safety considerations in the development of nanotechnology, offering a promising pathway for the creation of sustainable and safe nanomaterials that meet regulatory standards and public safety expectations. Future research should continue to explore similar approaches for other nanomaterials and refine the methodologies to balance functionality with safety and sustainability.

CRediT authorship contribution statement

Elena Cesa: Writing – original draft, Methodology, Investigation, Data curation, Conceptualization. **Anna Luisa Costa:** Writing – review & editing, Resources, Conceptualization. **Lara Faccani:** Investigation. **Dario Fornara:** Data curation. **Hulya Yilmaz:** Investigation. **Mustafa Culha:** Writing – review & editing, Resources, Conceptualization. **Sevin Adiguzel:** Investigation. **Gulnur Sener:** Investigation. **Nilay Cicek:** Investigation. **Tugba Muhlise Okyay:** Investigation. **Paola Ziosi:** Investigation. **Sébastien Artous:** Investigation. **Sébastien Jacquinot:** Investigation. **Arantxa Ballesteros:** Methodology, Investigation. **Javier Alcodori:** Investigation. **Ivone Pinheiro:** Investigation. **Laura Rodriguez-Lorenzo:** Investigation. **Begoña Espiña:** Writing – review & editing, Supervision, Investigation. **Filippo Marchetti:** Investigation, Writing – review & editing. **Anna Baldisserotto:** Supervision, Methodology. **Stefano Manfredini:** Writing – review & editing, Resources, Conceptualization. **Silvia Vertuani:** Writing – review & editing, Supervision, Conceptualization.

Informed consent statement

Not applicable.

Institutional review board statement

Not applicable.

Funding

This research was funded by Horizon Europe Framework Programme: Horizon 2020 and Horizon Europe, under grant agreements No. 953206 (SbD4Nano) and 101137324 (SUNRISE), respectively (Ambrosialab Accredited University of Ferrara Spinoff Company).

Declaration of competing interest

The authors declare the following financial interests/personal relationships which may be considered as potential competing interests: Stefano Manfredini reports that equipment, drugs, or supplies and travel were provided by Ambrosialab Accredited University Spinoff Company. Stefano Manfredini reports a relationship with Ambrosialab, Accredited Spinoff Company of the University of Ferrara that includes: equity or stocks, funding grants, speaking and lecture fees, and travel reimbursement. Silvia Vertuani reports a relationship with Ambrosialab, Accredited Spinoff Company of the University of Ferrara that includes: equity or stocks and travel reimbursement. Stefano Manfredini and Silvia Vertuani have filed patent #Italian patent application no. 102025000000321 issued to Assignee. Other authors, they declare that they have no known competing financial interests or personal relationships that could have appeared to influence the work reported in this paper.

Acknowledgments

The authors wish to thank Elisa Durini PhD for excellent technical assistance and Negar Eftekhari, Edi Simoni, and Cinzia Brenna, of the Microscopy Centre of the University of Ferrara for helpful assistance. The authors (S.M. and S.V.) wish also to thank CNR-ISSMC (A.L.C.) and Lamberti SpA (D.F.) for the support to the E.C. PhD grant.

Appendix A. Supplementary data

Supplementary data to this article can be found online at https://doi.org/10.1016/j.jcis.2025.138823.

Data availability

The original contributions presented in the study are included in the article/Supplementary Material, further inquiries can be directed to the corresponding author.

References

[1] C.M. Sayes, R. Wahi, P.A. Kurian, et al., Correlating nanoscale titania structure with toxicity: a cytotoxicity and inflammatory response study with human dermal fibroblasts and human lung epithelial cells, Toxicol. Sci. 92 (2006) 174–185, https://doi.org/10.1093/TOXSCI/KFJ197.
[2] A.D. Racovita, Titanium dioxide: structure, impact, and toxicity, Int. J. Environ. Res. Public Health 19 (2022), https://doi.org/10.3390/IJERPH19095681.
[3] S. Shabbir, MfeA Kulyar, Z.A. Bhutta, et al., Toxicological consequences of titanium dioxide nanoparticles (TiO_2NPs) and their jeopardy to human population, Bionanoscience 11 (2021) 621, https://doi.org/10.1007/S12668-021-00836-3.
[4] M.M. Rashid, P.F. Tavčer, B. Tomšič, Influence of titanium dioxide nanoparticles on human health and the environment, Nanomaterials 11 (2021), https://doi.org/10.3390/NANO11092354.
[5] M.G. Bianchi, M. Allegri, M. Chiu, et al., Lipopolysaccharide adsorbed to the biocorona of TiO_2 nanoparticles powerfully activates selected pro-inflammatory transduction pathways, Front. Immunol. 8 (2017), https://doi.org/10.3389/fimmu.2017.00866.
[6] F. Grande, P. Tucci, Titanium dioxide nanoparticles: a risk for human health? Mini Rev. Med. Chem. 16 (2016) 762–769, https://doi.org/10.2174/1389557516666160321114341.
[7] T. Ayorinde, C.M. Sayes, An updated review of industrially relevant titanium dioxide and its environmental health effects, J. Hazard. Mater. Lett. 4 (2023) 100085, https://doi.org/10.1016/J.HAZL.2023.100085.
[8] C.J. Querebillo, A review on Nano Ti-based oxides for dark and photocatalysis: from photoinduced processes to bioimplant applications, Nanomaterials 13 (2023), https://doi.org/10.3390/NANO13060982.
[9] Z. Luo, Z. Li, Z. Xie, et al., Rethinking nano-TiO2 safety: overview of toxic effects in humans and aquatic animals, Small 16 (2020), https://doi.org/10.1002/SMLL.202002019.
[10] T.G. Smijs, S. Pavel, Titanium dioxide and zinc oxide nanoparticles in sunscreens: focus on their safety and effectiveness, Nanotechnol. Sci. Appl. 4 (2011) 95, https://doi.org/10.2147/NSA.S19419.
[11] V.P. Chavda, D. Acharya, V. Hala, et al., Sunscreens: a comprehensive review with the application of nanotechnology, J. Drug Deliv. Sci. Technol. 86 (2023) 104720, https://doi.org/10.1016/J.JDDST.2023.104720.

[12] S. Ortelli, A.L. Costa, I. Zanoni, et al., TiO2@BSA nano-composites investigated through orthogonal multi-techniques characterization platform, Colloids Surf. B Biointerfaces 207 (2021) 112037, https://doi.org/10.1016/J.COLSURFB.2021.112037.
[13] M. Chaki Borrás, R. Sluyter, P.J. Barker, et al., Y2O3 decorated TiO2 nanoparticles: enhanced UV attenuation and suppressed photocatalytic activity with promise for cosmetic and sunscreen applications, J. Photochem. Photobiol. B 207 (2020) 111883, https://doi.org/10.1016/J.JPHOTOBIOL.2020.111883.
[14] A. Morlando, V. Sencadas, D. Cardillo, K. Konstantinov, Suppression of the photocatalytic activity of TiO2 nanoparticles encapsulated by chitosan through a spray-drying method with potential for use in sunblocking applications, Powder Technol. 329 (2018) 252–259, https://doi.org/10.1016/J.POWTEC.2018.01.057.
[15] J. Guo, H. van Bui, D. Valdesueiro, et al., Suppressing the photocatalytic activity of TiO2 nanoparticles by extremely thin Al2O3 films grown by gas-phase deposition at ambient conditions, Nanomaterials 8 (2018), https://doi.org/10.3390/NANO8020061.
[16] I. Furxhi, A. Costa, S. Vázquez-Campos, et al., Status, implications and challenges of European safe and sustainable by design paradigms applicable to nanomaterials and advanced materials, RSC Sustain. 1 (2023) 234–250, https://doi.org/10.1039/D2SU00101B.
[17] H.R. Ahmadi-Ashtiani, A. Baldisserotto, E. Cesa, et al., Microbial biosurfactants as key multifunctional ingredients for sustainable cosmetics, Cosmetics 7 (2020) 46, https://doi.org/10.3390/COSMETICS7020046.
[18] M. Hassanisaadi, Surfactin as a multifaceted biometabolite for sustainable plant defense: a review, J. Plant Pathol. 1–17 (2024), https://doi.org/10.1007/S42161-024-01645-9/FIGURES/2.
[19] I. Gugel, M. Vahidinasab, E.H. Benatto Perino, et al., Fed-batch bioreactor cultivation of *Bacillus subtilis* using vegetable juice as an alternative carbon source for lipopeptides production: a shift towards a circular bioeconomy, Fermentation 10 (2024) 323, https://doi.org/10.3390/fermentation10060323.
[20] H.-R. Ahmadi-Ashtiani, A. Baldisserotto, E. Cesa, S. Manfredini, H.S. Zadeh, M. G. Gorab, M. Khanahmadi, S. Zakizadeh, P. Buso, S. Vertuani, Microbial biosurfactants as key multifunctional ingredients for sustainable cosmetics, Cosmetics 7 (2020) 1–35.
[21] J.-M. Bonmatin, M. Genest, H. Labbé, M. Ptak, Solution three-dimensional structure of surfactin: a cyclic lipopeptide studied by 1H-nmr, distance geometry, and molecular dynamics, Biopolymers 34 (1994) 975–986.
[22] M. Blosi, A. Brigliadori, I. Zanoni, et al., *Chlorella vulgaris* meets TiO_2 NPs: effective sorbent/photocatalytic hybrid materials for water treatment application, J. Environ. Manage. 304 (2022) 114187, https://doi.org/10.1016/j.jenvman.2021.114187.
[23] S. Ortelli, A.L. Costa, Nanoencapsulation techniques as a "safer by (molecular) design" tool, Nano-Struct. Nano-Obj. 13 (2018) 155–162, https://doi.org/10.1016/j.nanoso.2016.03.006.
[24] F. Schreiber, Structure and growth of self-assembling monolayers, Prog. Surf. Sci. 65 (2000) 151–257, https://doi.org/10.1016/S0079-6816(00)00024-1.
[25] A.L. Costa, C. Galassi, R. Greenwood, α-Alumina-H_2O interface analysis by electroacoustic measurements, J. Colloid Interface Sci. 212 (2) (1999) 350–356, https://doi.org/10.1006/jcis.1998.6070.
[26] B.A. van Driel, P.J. Kooyman, K.J. van den Berg, et al., A quick assessment of the photocatalytic activity of TiO2 pigments — from lab to conservation studio!, Microchem. J. 126 (2016) 162–171, https://doi.org/10.1016/j.microc.2015.11.048.
[27] K.A. Jensen, M. Levin, Methods for testing dustiness, 2016.
[28] C. Dazon, O. Witschger, S. Bau, et al., Dustiness of 14 carbon nanotubes using the vortex shaker method, J. Phys. Conf. Ser. 838 (2017) 012005, https://doi.org/10.1088/1742-6596/838/1/012005.
[29] I. Pinheiro, M. Quarato, A. Moreda-Piñeiro, et al., Acute aquatic toxicity to zebrafish and bioaccumulation in marine mussels of antimony tin oxide nanoparticles, Nanomaterials 13 (14) (2023) 2112, https://doi.org/10.3390/nano13142112.
[30] C.B. Kimmel, W.W. Ballard, S.R. Kimmel, et al., Stages of embryonic development of the zebrafish, Dev. Dyn. 203 (1995) 253–310, https://doi.org/10.1002/aja.1002030302.
[31] Dimitrovska Cvetkovska A, Manfredini S, Ziosi et al. (2017) Factors affecting SPF in vitro measurement and correlation with in vivo results. Int. J. Cosmet. Sci. 39 310–9 doi:https://doi.org/10.1111/ics.12377.
[32] The Commission of the European Communities, COMMISSION RECOMMENDATION of 22 September 2006 on the efficacy of sunscreen products and the claims made relating thereto. (Notified Under Document Number C(2006) 4089), Off. J. Eur. Union 265 (2006) 39–43.
[33] S. Mohammadi-Jam, K.E. Waters, R.W. Greenwood, A review of zeta potential measurements using electroacoustics, Adv. Colloid Interface Sci. 309 (2022) 102778, https://doi.org/10.1016/J.CIS.2022.102778.
[34] A.L. Costa, B. Ballarin, A. Spegni, et al., Synthesis of nanostructured magnetic photocatalyst by colloidal approach and spray-drying technique, J. Colloid Interface Sci. 388 (2012), https://doi.org/10.1016/j.jcis.2012.07.077.
[35] H.S. El-Sheshtawy, I. Aiad, M.E. Osman, et al., Production of biosurfactant from bacillus licheniformis for microbial enhanced oil recovery and inhibition the growth of sulfate reducing bacteria, Egypt. J. Pet. 24 (2) (2015) 155–162, https://doi.org/10.1016/j.ejpe.2015.05.005.
[36] A. León, P. Reuquen, C. Garín, et al., FTIR and Raman characterization of TiO_2 nanoparticles coated with polyethylene glycol as carrier for 2-methoxyestradiol, Appl. Sci. 7 (2017) 1–9, https://doi.org/10.3390/app7010049.
[37] A. Nilchi, S. Janitabar-darzi, A.R. Mahjoub, S. Rasouli-garmarodi, New TiO_2/SiO_2 nanocomposites — phase transformations and photocatalytic studies, Colloids Surf., A Physicochem. Eng. Asp. 361 (2010) 25–30, https://doi.org/10.1016/j.colsurfa.2010.03.006.
[38] H. Jensen, J.H. Pedersen, J.E. Jørgensen, et al., Determination of size distributions in nanosized powders by TEM, XRD, and SAXS, J. Exp. Nanosci. 1 (2006) 355–373, https://doi.org/10.1080/17458080600752482.
[39] C. Marinescu, A. Sofronia, C. Rusti, et al., DSC investigation of nanocrystalline TiO2 powder, J. Therm. Anal. Calorim. 103 (2011) 49–57, https://doi.org/10.1007/S10973-010-1072-6.
[40] A.E. Slobozeanu, S.E. Bejan, I.A. Tudor, et al., A review on differential scanning calorimetry as a tool for thermal assessment of nanostructured coatings, Manuf. Rev. (Les. Ulis.) 8 (2021) 1, https://doi.org/10.1051/MFREVIEW/2020038.
[41] R. Geng, Y. Ren, R. Rao, et al., Titanium dioxide nanoparticles induced hela cell necrosis under uva radiation through the ros-mptp pathway, Nanomaterials 10 (2020) 1–15, https://doi.org/10.3390/NANO10102029.
[42] M. Battistin, E. Durini, V. Dissette, et al., Synthesis and characterization of new multifunctional self-boosted filters for UV protection: ZnO complex with dihydroxyphenyl benzimidazole carboxylic acid, Molecules 24 (2020) 1–24, https://doi.org/10.3390/MOLECULES24244546.
[43] M. Battistin, V. Dissette, A. Bonetto, et al., A new approach to UV protection by direct surface functionalization of TiO2 with the antioxidant polyphenol dihydroxyphenyl benzimidazole carboxylic acid, Nanomaterials 10 (2020) 231, https://doi.org/10.3390/NANO10020231.
[44] B. Milićević, V. Đorđević, D. Lončarević, et al., Charge-transfer complex formation between TiO2 nanoparticles and thiosalicylic acid: a comprehensive experimental and DFT study, Opt. Mater. (Amst.) 73 (2017) 163–171, https://doi.org/10.1016/J.OPTMAT.2017.08.011.
[45] Caldeira C, Aguirre G, Tosches I, et al Safe and Sustainable by Design chemicals and materials Application of the SSbD framework to case studies. doi:https://doi.org/10.2760/769211.
[46] K. Bhattacharya, M. Davoren, J. Boertz, et al., Titanium dioxide nanoparticles induce oxidative stress and DNA-adduct formation but not DNA-breakage in human lung cells, Part. Fibre Toxicol. 6 (2009), https://doi.org/10.1186/1743-8977-6-17.
[47] C.S. Park, K.S. Choi, I.W. Park, et al., Autophagy in RAW264.7 cells treated with surface-functionalized graphene oxides, J. Nanomater. (2015), https://doi.org/10.1155/2015/704789.
[48] G. Tortini, P. Ziosi, E. Cesa, S. Molesini, E. Baldini, D. De Lucia, C. Rossi, E. Durini, S. Vertuani, S. Manfredini, Criticisms in the development of high-protection and broad-Spectrum "natural/organic" certifiable sunscreen, Cosmetics 9 (2022) 1–18, https://doi.org/10.3390/cosmetics9030056.
[49] J. Jiménez, P. Leret, C.M. Álvarez-docio, J.F. Fernández, Enhancement of UV absorption behavior in ZnO – TiO2 composites Bol. la Soc, Esp. Ceram. y Vidr. 5 (2016) 55–62, https://doi.org/10.1016/j.bsecv.2016.01.004.
[50] M. Pelizzo, E. Zattra, P. Nicolosi, A. Peserico, D. Garoli, M. Alaibac, In vitro evaluation of sunscreens : an update for the clinicians, Int. Sch. Res. Netw. Dermatol. 1–4 (2012), https://doi.org/10.5402/2012/352135.